Impact of ocean heat transport on the natural and forced variability of Arctic sea-ice in the GFDL CM2-O model suite

Marine Decuypère[1], L. Bruno Tremblay[1], Carolina O. Dufour[1]

[1]Department of Atmospheric and Oceanic Sciences, McGill University, Montréal, Québec, Canada

Key Points:

- Ocean heat transport into the Arctic does not systematically increase with horizontal resolution.
- The eddying models show a stronger response to climate change than the non-eddying model.
- Flow partitioning in the northern North Atlantic and location of deep convection centers are key to the heat transport into the Arctic.

Corresponding author: Marine Decuypère, `marine.decuypere@mail.mcgill.ca`

Abstract

A recent study links an increase in the horizontal resolution of ocean models to improved representations of Arctic sea-ice and Ocean Heat Transport (OHT, Docquier et al., 2019). Here, the impact of horizontal resolution on meridional OHT and sea-ice is investigated over a broader range of resolutions, using the GFDL CM2-O climate model suite (1.0 °, 0.25°, and 0.1°) in both preindustrial control and climate change simulations. Results show a direct link between OHT and sea-ice extent (SIE) in the Arctic. This link, however, is not monotonic with spatial resolution. While OHT increases and SIE decreases from the Low to the Medium resolution models, the reverse is true from the Medium to the High resolution models. Differences in OHT and SIE between the three models mostly arise from the preindustrial state. As the spatial resolution increases, the Irminger Current is favored at the expense of the North Atlantic Drift. This rerouting of water to the Western side of Greenland results in less heat delivered to the Arctic in the High resolution model than in its Medium counterpart. As a result, the Medium resolution model is in best agreement with observed SIE and Atlantic OHT. Concurrent with the change in the partitioning in volume is a change in deep convection centers from the Greenland-Irminger-Norwegian Seas in the Low resolution model to the Labrador Sea in the High resolution model. Results suggest a coupling between OHT into the Arctic and deep convection in the North Atlantic.

Plain Language Summary

The ocean is one of the main drivers of sea ice loss and variability in the Arctic. A recent study links an increase in the horizontal resolution of ocean models to improved representations of Arctic sea-ice and ocean heat transport (Docquier et al., 2019). Here, the impact of horizontal resolution on the natural variability and response to climate change of ocean heat transport and sea ice is investigated in a suite of three climate models of different horizontal resolutions in the ocean. Results show a direct link between ocean heat transport and sea ice extent, however the ocean heat transport into the Arctic does not systematically increase with horizontal resolution as expected from (Docquier et al., 2019). Under climate change, the medium resolution model shows the strongest ocean heat transport and lowest sea ice extent of the suite due to its natural (preindustrial) mean state rather than to its response to carbon dioxide increase. The representation of current pathways is found to differ greatly between the three models in the northern North Atlantic, impacting the penetration of the relatively warm Atlantic waters into the Arctic. This difference in currents between models is concurrent with a difference in the location of deep convection in the North Atlantic.

1 Introduction

Model developments aimed at improving climate projections are generally focused on refining spatial resolution, or advancing parameterizations. The development of parameterizations can target specific processes, requires less workforce, and is simpler to implement in the standard 7-year cycle of the Intergovernmental Panel on Climate Change (IPCC). Refining spatial resolution, on the other hand, is costly both numerically (the total integration time increases by a factor of at least 8 for each doubling of horizontal spatial resolution; Flato, 2011) and in terms of workforce since all remnant parameterizations must be recalibrated as a function of newly resolved spatial scales, as the assumptions made for parameterizations do not hold at finer resolutions (Molinari & Dudek, 1992).

For these reasons, climate groups have mainly focused on new or improved parameterizations of sub-grid scale processes in recent decades (e.g. Fox-Kemper et al., 2011; Brankart, 2013; Jansen et al., 2015), whereas the spatial resolution of the ocean component in global climate models has remained mostly the same (around 1°) in the last several rounds of the Coupled Model Intercomparison Project (CMIP). In the context of Arctic climate, the new parameterizations include surface melt pond (M. M. Holland et al., 2012), ice thickness distribution (Bitz et al., 2001; Ungermann et al., 2017), lateral melt (Tsamados et al., 2015; Smith et al., 2021) and ice-ocean heat exchange (Shi et al., 2020), among others. These developments have led to significant improvements in the simulation of the mean state and variability (forced and natural) of the ice-ocean system, including the sea ice thickness distribution (Bitz et al., 2002; Bitz & Roe, 2004; Shi et al., 2020), and sensitivity of the sea ice cover to increased carbon dioxide (CO_2) concentration (M. M. Holland et al., 2006; Stroeve et al., 2014; Jahn et al., 2016; Auclair & Tremblay, 2018).

Recently, climate groups have started to explore the sensitivity of the climate system to an eddying ocean. For instance, the High Resolution Model Intercomparaison Project (HighResMIP) proposed a common protocol for high resolution model simulations under the umbrella of the World Climate Research Program (WCRP; Haarsma et al., 2016). In the early 2010s, both the Geophysical Fluid Dynamics Laboratory (GFDL) and the National Center for Atmospheric Research (NCAR) have developed a climate model with an ocean component at 0.1° for century scale simulations of the past, present and future climate (Delworth et al., 2012; Kirtman et al., 2012). Using the GFDL 0.1° model, Griffies et al. (2015) find that mesoscale eddies play a significant role in the upward vertical heat transport and ocean heat uptake, and that this model yields a generally more accurate representation of global ocean temperature and heat budget. Using the same model, Saba et al. (2016) show that a refined resolution provides a more realistic representation of the Northwest Atlantic Shelf circulation, and a higher warming rate to increased CO_2 forcing. Dufour et al. (2017) show that this same model enables the formation of polynyas in the Weddell Sea compared to a coarser resolution model, thanks to a stronger stratification in the Southern ocean and a better representation of transient eddies and topographical features. Drake et al. (2018) find that this fine resolution model leads to a significantly shorter advective upwelling time scale of Circumpolar Deep Waters in the Southern Ocean compared to the coarser resolution configurations, because of eddy variability, thus highlighting the role of mesoscale eddies in large scale circulation time scale.

Studies using global climate models and ocean-only models have also investigated the effect of refining spatial resolution on the sub-polar gyre and Atlantic water pathways in the northern North Atlantic, Irminger Sea, Labrador Sea and Baffin Bay in the context of ice shelf-ocean interactions and increased rate of advance of marine glaciers (Myers et al., 2007; Straneo & Heimbach, 2013). Marzocchi et al. (2015) find that a high resolution model (1/12° resolution) leads to an improved representation of the subpolar gyre and a better representation of Labrador Sea Water formation and variability compared to the 1° and 1/4° versions of the same model. Koenigk et al. (2021) find that increasing the ocean model resolution from 1° to 1/4° leads to an increase in deep mixing in the Labrador Sea and draw a direct link between the subpolar gyre strength, surface ocean salinity and depth of convection. García-Quintana et al. (2019) find less formation of Labrador Sea Water in a 1/12° model compared to a 1/4° model, due to a shallowing of the mixed layer and a smaller area of deep convection. Pennelly and Myers (2020) study the impact of resolution (from 1/4° to 1/12° to 1/60°) on Labrador Sea circulation, and find that the mixed layer depth in the Labrador sea is shallower as the resolution increases thanks to an increase in eddy kinetic energy, and that Labrador Sea Waters density is better represented in the 1/60° model.

Several studies showed that an increase in resolution leads to an increase in mid-latitude meridional ocean heat transport (OHT) in general (Griffies et al., 2015; Hewitt et al., 2016) and in the Atlantic Ocean in particular (Grist et al., 2018). A better representation of OHT is needed to improve projections of sea ice extent (SIE), as the ocean is one of the main drivers of sea ice loss and variability in the Arctic (Bitz et al., 2005). Indeed, in recent years, an increase in the Barents Sea Opening OHT led Atlantic Waters to penetrate deeper into the Eurasian Basin (Smedsrud et al., 2010), a process known as the Atlantification of the Arctic (Årthun et al., 2012; Polyakov et al., 2017). This was accompanied by a weakening of the stratification in the Eurasian Basin and enhanced vertical heat fluxes from Atlantic Waters (Polyakov et al., 2017), and a limited winter sea ice growth in the Barents Sea (Barton et al., 2018). Variability in Atlantic OHT is responsible for the interannual variability SIE in the Barents Sea (Årthun et al., 2012, 2019). The impact of the Atlantic multidecadal variability on the Arctic SIE has been highlighted especially for Barents Sea sea temperature and ice extent (Drinkwater et al., 2014; Årthun et al., 2019; Mette et al., 2021) and the Greenland Ice Sheet (Drinkwater et al., 2014). Pacific Waters also play a key role in sea ice loss : for instance, Woodgate et al. (2010) argued that a doubling of ocean heat flux through the Bering Strait between 2001 and 2007 was responsible for a third of the 2007 seasonal sea ice loss. Finally, correlation between OHT and SIE is shown at interannual and decadal time scales during rapid decline events in the Community Earth System Model - LE (Auclair & Tremblay, 2018; Li et al., 2017).

While the impact of spatial resolution on global scale circulation patterns has been discussed, relatively fewer studies focus on the impact of resolution on OHT and SIE variability in the Arctic Ocean. Griffies et al. (2015) find a lower poleward OHT in the coarse resolution model (1° resolution) than in the finer resolution models (1/4° and 1/10° resolution), due to weaker sub-tropical and sub-polar gyre transports. Furthermore, Hewitt et al. (2016) find that increased ocean and atmosphere resolutions (from 1/4° to 1/12°, and 60 km to 25 km respectively) with higher coupling frequency lead to an enhanced poleward OHT and warmer ocean surface in the North Atlantic, and lower SIE. A recent study by Docquier et al. (2019) shows that, in the CMIP6 models participating in the High Resolution Model Intercomparison Project, the increase of spatial resolution from 1° to 1/4° yields a larger Atlantic OHT and lower sea ice extent and volume. Furthermore, while the models exhibit strong correlations between the Atlantic OHT and the SIE variability in the Barents, Kara and Greenland Seas, the correlations do not increase uniformly with resolution across the models studied.

In this paper, we use the GFDL CM2-O model suite which comprises three climate models that are identical to one another in all aspects except for the horizontal resolution of the ocean component and the absence of mesoscale eddy parameterizations in models where eddies are partly resolved. We investigate the impact of refining the horizontal grid spacing of the ocean component on OHT in the Arctic, SIE and their relationship. We find that the magnitude of OHT and sea ice are strongly correlated on (multi) decadal time scales ; however the links between OHT and SIE at interannual scale differ between models. While the increase from the 1° resolution to the 1/4° resolution does lead to an increase in OHT and decrease in SIE (in agreement with Docquier et al., 2019), the increase from the 1/4° resolution to the 1/10° leads to an opposite response. In addition, the change in resolution impacts the partitioning of North Atlantic heat transport thus resulting in different sea ice conditions.

The paper is structured as follows. In section 2, we present the GFDL CM2-O model suite and the simulations. In section 3, we describe the methods used to analyse the model output. In section 4, we present the SIE and OHT mean states, their response to an idealised climate change simulation as well as the impact of OHT on SIE. In section 5, we discuss the differences in the ocean circulation in the North Atlantic across the model suite and their potential impact on the OHT and sea ice.

2 Model Description and Simulations

2.1 The CM2-O Model Suite

In this study, we use the GFDL CM2-O model suite that comprises three models differing only in the horizontal grid spacing of their ocean component: CM2-1deg (1°), CM2.5 (0.25°), CM2.6 (0.1°) (Delworth et al., 2012; Griffies et al., 2015).

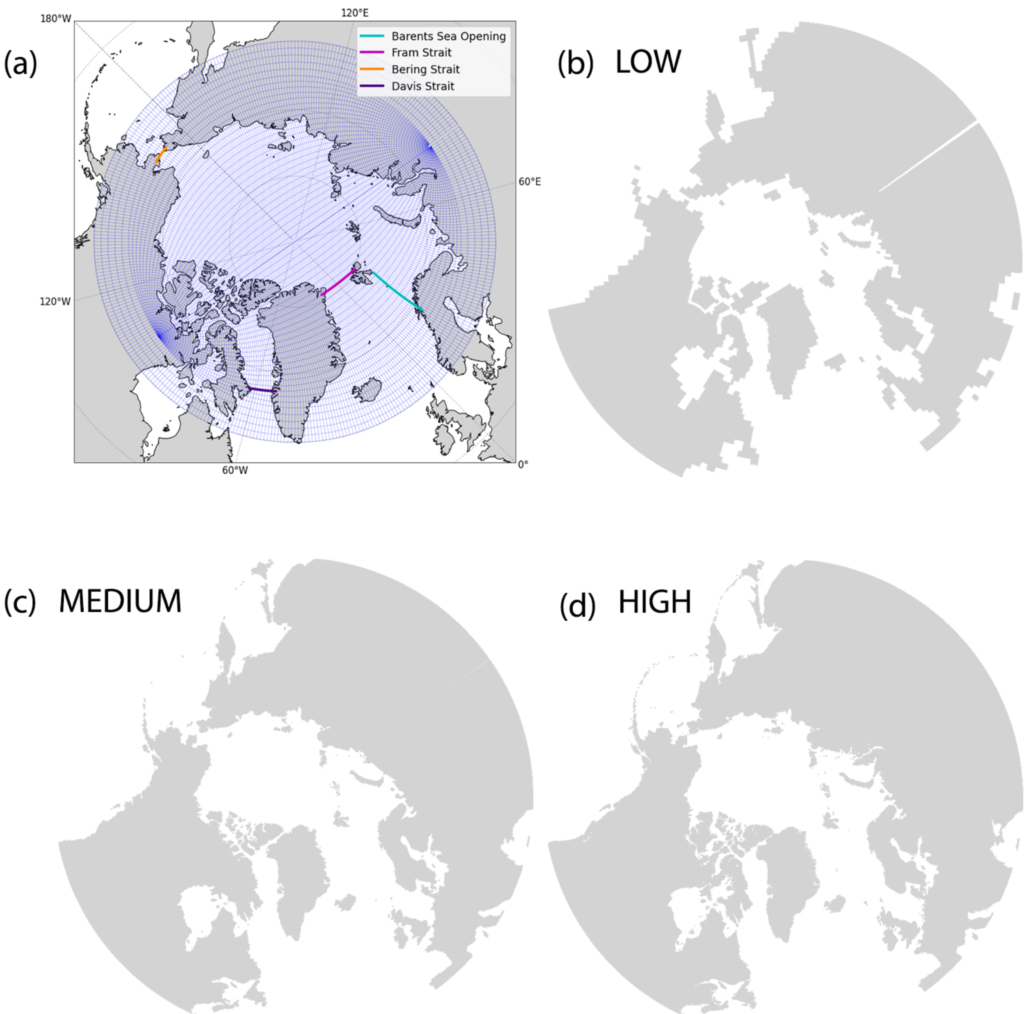

Figure 1. (a) Arctic model domain and tripolar grid in CM2-1deg (Low resolution model). The main gates used in the study are: the Fram Strait (pink), the Barents Sea Opening (cyan) the Bering Strait (orange) and the Davis Strait (purple). The coastlines are drawn from observations. Landmasks in the (b) Low (c) Medium and (d) High resolution model.

The ocean component is the version 5 of the Modular Ocean Model (MOM5; Griffies et al., 2015) run with volume-conserving Boussinesq kinematics. The model uses a tripolar grid, with one pole at the South Pole, and two poles placed over northern Canada and Russia (Fig. 1 a; Murray, 1996). The ocean model is run with a z^* geopotential vertical coordinate (meaning that grid cell thickness is time dependent) and 50 layers in the vertical. At rest, the thickness of the layers ranges from 10 m in the first 250 m to 210 m at the bottom. The thickness of bottom cells is adjusted to match topography using

Table 1. Summary of key differences between the Low, Medium and High resolution models of the CM2-O suite. The SIE trends are calculated over the 80 years of the CC simulation, and the observed trends are computed over the equivalent years of CO_2 concentrations (1979-2019; Fetterer et al., 2017). Note that the simulated SIE trends are linear over the 80 year period. Interannual variability is the standard deviation relative to a five-year running mean. OHT into the Arctic Ocean is defined as positive. The observed OHTs are from Beszczynska-Möller et al. (2011). The model OHT is the average over the years with equivalent CO_2 concentration to the observation periods.

	Low	Medium	High	Observations
Nominal horizontal resolution (°)	1	0.25	0.1	-
Horizontal resolution at 65°N (km)	46 x 111	11 x 11	4 x 4	-
Mesoscale eddy parameterization	Yes	No	No	-
March SIE trend (million km^2/model decade)	-0.1	-0.5	-0.5	-0.9
September SIE trend (million km^2/model decade)	-0.3	-0.6	-0.6	-1.6
March SIE interannual variability (million km^2)	0.24	0.18	0.23	0.23
September SIE interannual variability (million km^2)	0.41	0.36	0.32	0.44
Fram Strait OHT (TW)	17	37	23	$30-42$
Bering Strait OHT (TW)	1	5	3	$10-20$
Barents Sea Opening OHT (TW)	3	76	38	$50-70$

the partial cell method (Pacanowski & Gnanadesikan, 1998). The model uses the piecewise parabolic method for the advection scheme (Delworth et al., 2012), and the non-local K-profile parameterization for vertical mixing (Large et al., 1994). CM2-1deg includes the Ferrari et al. (2010) modified version of the Gent and McWilliams mesoscale eddy parameterization (Gent et al., 1995) with a maximum diffusivity of 1200 m^{2}s^{-1} as in Griffies et al. (2015) compared with 800 m^{2}s^{-1} in the ESM2M Earth System Model (Dunne et al., 2012). CM2.5 and CM2.6 enable some explicit representation of the mesoscale, though incomplete, and do not use a mesoscale eddy parameterization (Griffies et al., 2015). The resolution needed to resolve the baroclinic deformation radius in the Arctic ranges from 1/12° in the Central Arctic to 1/50° in the shallow waters near the coast (see Fig.2 of Hallberg, 2013). All three models use the submesoscale mixed layer eddy parameterization of Fox-Kemper et al. (2011). Key characteristics of the models are summarized in Table 1. From here after, we will refer to the CM2-1deg, CM2.5 and CM2.6 models as the *Low* (1°), *Medium* (0.25°) and *High* (0.1°) resolution models, respectively.

In the High resolution model, the refined horizontal resolution allows for a better representation of the Gulf of Ob in the Kara Sea and of the Canadian Arctic Archipelago (Fig. 1 b-d). Key differences between the High resolution model and the Medium and Low resolution models also include the resolution of the Alpha and Lomonosov ridges, the Barents Sea and the steepness of the continental slopes. In the Medium resolution model, the Victoria Strait, the Coronation Gulf, the Prince Regent Inlet and the Foxe Basin are closed. In the Low resolution model, the Fury and Hecla Strait connecting the Gulf of Boothia and Foxe Basin is closed. In contrast, all these basins and straits remain open in the High resolution model.

The sea ice component is the GFDL Sea Ice Simulator (SIS) which uses a three-layer Semtner thermodynamic model (one layer of snow, two layers of ice) with five ice-thickness categories (Semtner, 1976; Winton, 2000; Delworth et al., 2006) and a brine pocket parameterization (Bitz & Lipscomb, 1999). The model uses the same tripolar grid as the ocean component (Dunne et al., 2012). The dynamic component of the sea ice model uses the elastic-viscous-plastic rheology of Hunke and Dukowicz (1997). The maximum value for albedos are set to 0.85 for snow on ice and 0.68 for bare sea ice (Delworth et al., 2012).

The atmospheric component is the GFDL AM2.1 (Atmospheric Model 2.1). AM2.1 is run on a "cubed-sphere" grid with a horizontal resolution of 50 km and 32 vertical levels (Delworth et al., 2012), compared with 200 km and 24 levels in the GFDL CM2.1 described in Delworth et al. (2006). The advective terms are calculated with a modified Euler backward scheme (Kurihara & Tripoli, 1976). The atmospheric physics module is the GFDL AM2-LM2 model (Anderson et al., 2004) that includes three prognostic tracers for clouds: cloud liquid, cloud ice and cloud fraction. Finally, the suite uses the land component LM3 (Land Model 3) with a drainage route from Milly et al. (2014). More details about the suite or individual models' performance can be found in Delworth et al. (2012) and Griffies et al. (2015).

2.2 Simulations

We analyse a pre-industrial control run and a climate change run for each model, hereafter referred to as *CTRL* and *CC*, respectively. The CTRL simulation is run for 200 years with constant globally averaged CO_2 concentration of 286 ppmv corresponding to 1860. All models started from the same initial conditions. The CC run branches off from the control run at year 121 with an atmospheric CO_2 concentration increasing at 1% per year over 80 years leading to a doubling of CO_2 levels after 70 years (year 190 of the simulation). Only one ensemble member was run for each of the model of the suite due to the high computational and storage cost of the high-resolution model. In the following, we refer to the period from the beginning of the second decade to the middle of the third decade of the CC run as the "historical period", with CO_2 concentrations corresponding to the pre-satellite era (1950-1979). The CO_2 concentration during the satellite record (1979-2021) ranges from 370 to 415 ppmv which corresponds to the years 145 to 158 of the CC simulations, i.e. from the second half of the third decade to the fourth decade.

3 Method

The total Ocean Heat Transport (hereafter referred to as OHT) diagnostic in the CM2-O suite is calculated online at each time step as $\rho_0 c_p U \Theta dS$ where ρ_0 is the constant Boussinesq reference density (=1035 kg m^{-}3), c_p is the ocean heat capacity (=3992.1 J kg^{-}1 K^{-}1), U is the zonal or meridional ocean velocity, Θ is the potential temperature, and dS is the surface of the grid cell normal to the flow. The OHT at each gate is calculated by integrating the monthly or yearly averaged OHT across the gate and the full water column. Each gate is located on the same constant latitude or longitude grid points in all the models, and is defined from the Low resolution model for simplicity (Fig. 1). We find that the positioning of the gates can have a minor impact on the magnitude of the OHT, but the changes are uniform across the models and within the ranges of observation errors at the gates (not shown). Furthermore, the positioning has a negligible impact on the variability (not shown). We analyse monthly mean output from the last 80 years of each simulation, except for the mass and heat transports of the High resolution model where we use yearly means due to storage constraints. The interannual variability is defined as the variability around the five-year running mean.

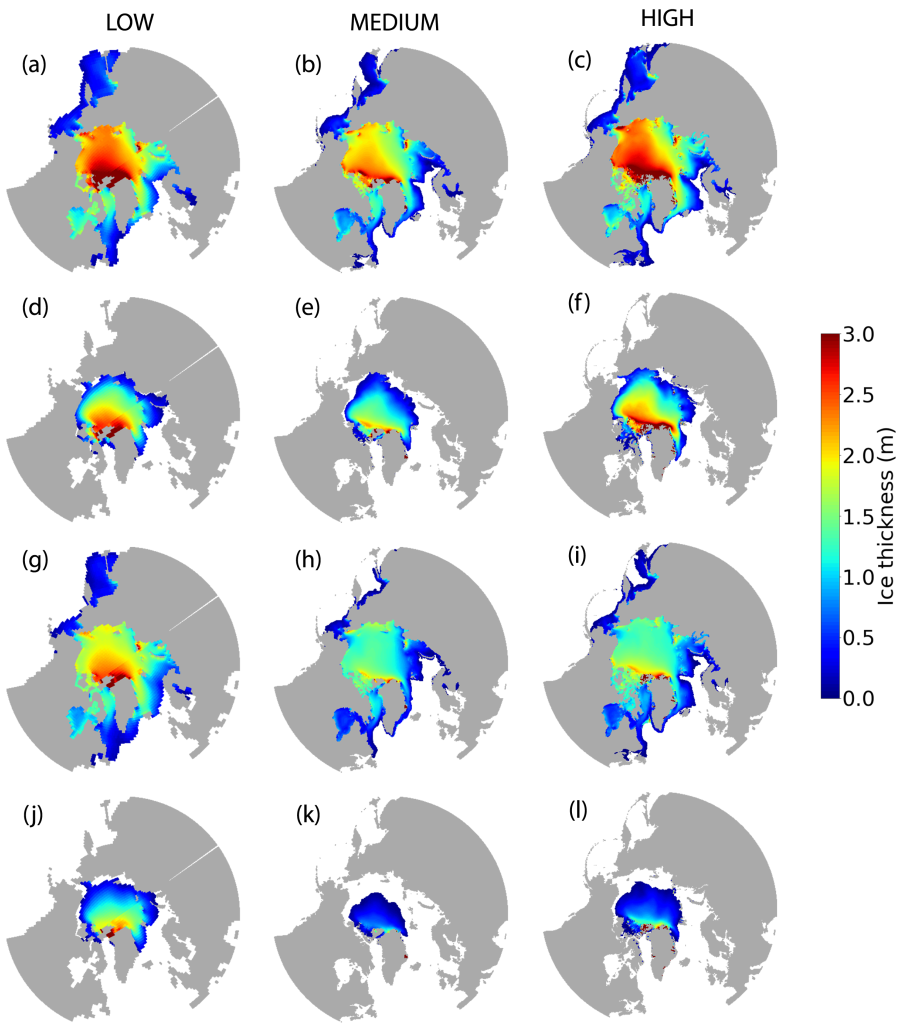

Figure 2. Sea ice thickness in the CC simulation averaged over the second decade (a-f) and the last decade (g-l) in March (a-c and g-i) and September (d-f and j-l) for the Low, Medium and High resolution models. The thicker ice reaches 4.5 m which is within realistic values, and some areas have an accumulation of anomalously thick ice due to the ice being trapped in the models (3 km thickness on the coast of Greenland for instance)

4 Results

4.1 Mean Arctic Ocean Climate over the Historical Period

4.1.1 Sea Ice Extent and Thickness

Over the historical record, all three models reproduce the pan-Arctic winter sea ice thickness distribution with thicker ice on the Canadian side and thinner ice on the Eurasian side of the Arctic, and an east-west asymmetry north of the Canadian Arctic Archipelago (Fig. 2 a-c). The winter sea ice thickness in the Low and High resolution models is in general agreement with submarine observations (Bourke & Garrett, 1987), except along the Alaskan coastline where thicker ice is present in models, indicative of a small bias in the location of the Arctic High. In the Medium resolution model, the sea ice is too thin by a few meters in the Canada Basin, and has a thick bias along the Alaskan coastline similarly to the other models. In the High and Low resolution models, the thicker ice in the East Siberian Sea is typical of climate models, where easterly winds interact with Wrangle Island and the New Siberian Islands (DeWeaver & Bitz, 2006). In the summer, the sea ice thickness is again in general agreement with observations in the Low and High resolution models, and too thin in the Medium resolution model (Fig. 2 d-f).

These thickness anomalies have an impact on the summer SIE. In the Low and High resolution models, the high bias in summer SIE is associated with an absence of sea ice melt in all peripheral seas, in part due to winter sea ice thickness anomalies in the western Arctic (Figs. 2 and 3). In the Medium resolution model, the minimum SIE is in excellent agreement with submarine and early satellite observations (Fig. 3). In the winter, there is a high bias in SIE in the Low and High resolution models which is primarily found in the Bering and Greenland Seas, suggesting a weaker subpolar gyre in both the northern North Pacific and Atlantic (Figs. 2 and 3). In the Medium resolution model, the winter SIE is in very good agreement with observations (Fig. 3).

The September and March SIE of the Medium resolution model are also in very good agreement with observations over the satellite era (1979-2019), with a small underestimation for September SIE, mostly in the Greenland and Barents Seas (Figs. 3 and 4). Conversely, in the Low and High resolution models, the September and March SIE (~ 9 and ~ 19 million km^2) are too large by about ~ 1 to 3 million km^2 in September and 3 million km^2 in March. While the September total SIE is realistic in the Medium resolution model, the spatial extent is too extensive in the East Siberian sea and too retreated in the Atlantic sector when compared to the satellite record (Fig. 4). In the Low resolution model, the September SIE is too large in all three sectors of the Arctic (Fig. 4). The High resolution model sea ice is too extensive in the Pacific and Eurasian sectors and in good agreement with the observations in the Atlantic sector (Fig. 4). While the Medium resolution model simulates the correct SIE, it does so with a much thinner ice cover throughout the simulation. Conversely, the Low and High resolution models simulate the correct sea ice thickness at the expense of the SIE representation.

The interannual variability of SIE is in good agreement with observations in all three models (see Table 1), though it is slightly underestimated in September. The increase in interannual variability observed during the transition to a seasonally ice-free Arctic is entirely missing in all the models (not shown, Desmarais & Tremblay, 2021). The decadal variability of SIE is larger than observations in September across the model suite, and in March for the Low resolution model (see Fig 3).

4.1.2 Ocean Heat Transport

During the observational period (1998-2007, depending on the gate studied, corresponding to the end of the third decade and the beginning of the fourth decade in the models), the Medium resolution model has a total OHT of 112 TW into the Arctic and is in good agreement with observations in the Fram Strait and Barents Sea Opening though the modelled OHT is slightly overestimated in the latter (see Table 1). The Low resolution model greatly underestimates the total OHT, with little heat entering the Arctic through the Barents Sea Opening and Bering Strait (3 TW and 1 TW respectively; Table 1). The OHT through the Fram Strait is also underestimated, by at least 13 TW. This lack of heat transport is also evident in the Arctic temperature maximum showing less Atlantic waters intrusion onto the Barents Sea shelf in the Low Resolution model compared to the other two models (see Fig. 8). The heat transport across the Barents Sea Opening is only 30% of that of the Community Earth System Model - Large Ensemble (CESM-LE) model for the same nominal resolution (Auclair & Tremblay, 2018) suggesting that its coarse resolution is not the only cause of this weak OHT. In the High resolution model, the OHTs in the Fram Strait and Barents Sea Opening are underes-

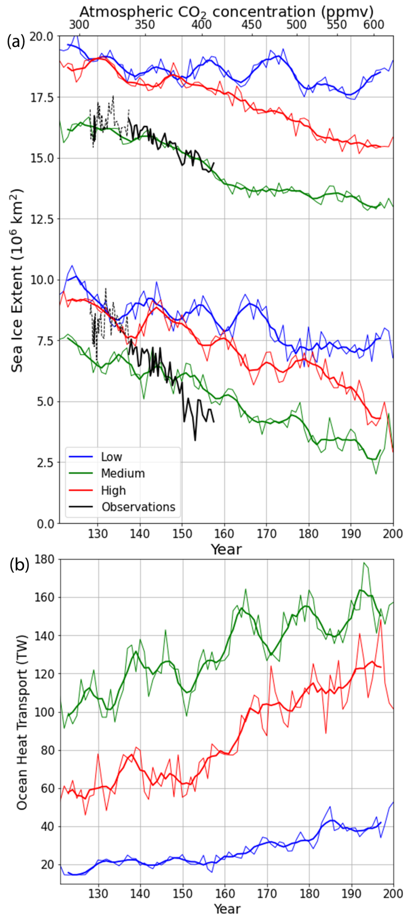

Figure 3. a) Observed March and September SIE between 1930 and 1979 from the historical record (dashed black line, Walsh et al., 2019) and between 1979 and 2019 from the satellite record (thick black line, Fetterer et al., 2017), and simulated March and September SIE (thin lines) and five-year running mean (thick lines) and b) Yearly mean total OHT into the Arctic as the sum of Barents Sea Opening, Fram Strait and Bering Strait OHT (thin lines) and five-year running mean (thick lines) as a function of time (model years; bottom axis) and CO_2 concentration (top axis) in the CC run for the Low, Medium and High resolution models. Note that the observations are plotted with respect to the CO_2 concentration for comparison with the models. The SIE is calculated as the area of grid cells where the sea ice concentration exceeds 15%.

timated by at least 7 TW and 12 TW respectively (Table 1). All models strongly underestimate the OHT across the Bering Strait with the modelled OHTs reaching at most 50% of the observational estimates.

Over the observational period, the Medium resolution model remains the closest to the observational estimates of OHT and SIE (Table 1 and Fig. 3). Of the three models, that model also carries the most heat into the Arctic ($\sim 50\%$ more heat than the High resolution model). Both the Low and High resolution models underestimate the OHT and overestimate SIE over the observational period, with the High resolution model showing significantly greater OHT but only slightly lower SIE than its lower resolution counterpart. Hence, in the CM2-O model suite, the greater the OHT, the lower the SIE, which suggests a major impact of OHT on SIE.

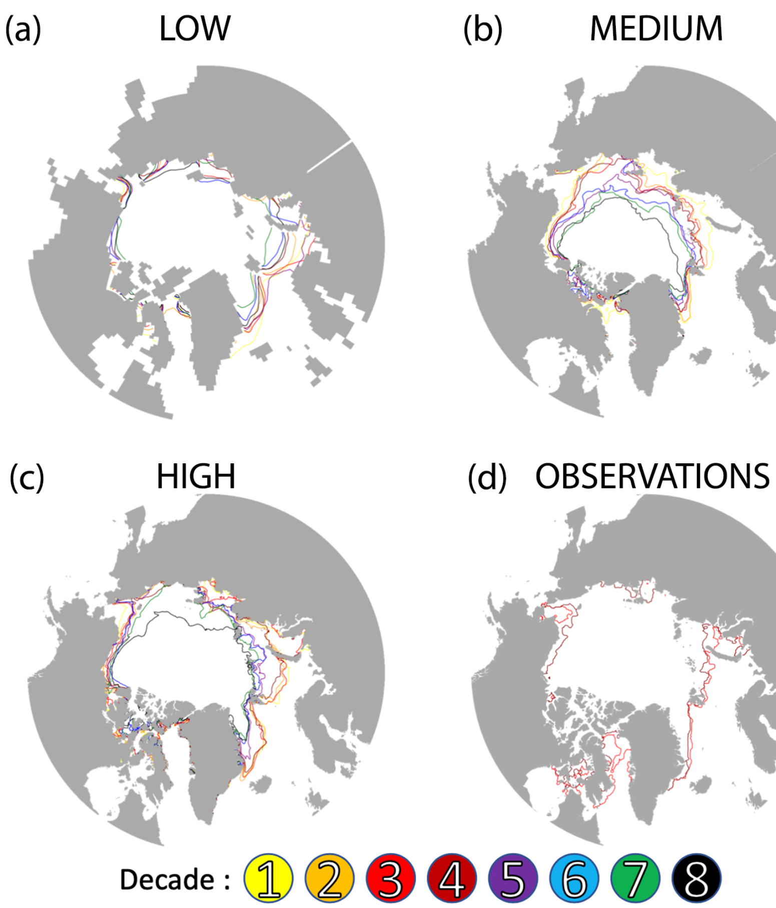

Figure 4. SIE averaged over each decade of the CC simulation for the (a) Low , (b) Medium and (c) High resolution models, and for (d) observations over the satellite record. The first decade begins with model year 121 while the last decade ends with model year 200. The satellite era corresponds to 3 and 4 according to equivalent CO_2 levels.

4.2 Impact of OHT on SIE at a Pan-Arctic Scale

In response to the CO_2 forcing, all models show a linear decline in SIE with a clear decadal to multidecadal signal super-imposed (Fig. 3, Table 1). The trends in the minimum SIE in the Medium and High resolution models are around -0.6×10^6 km^2/ model decade (significant at the 95% confidence level), much smaller than the observed trend of -1.6 million km^2/model decade in the satellite era. We note that, even without adjusting the observed trend to the CO_2 concentration in the model simulation, the trend in observations is still higher than in the models (-0.8 million km^2/decade; not shown). The underestimation of sea ice decline in the CM2-O suite is common among climate models (Stroeve et al., 2012; Notz & SIMIP Community, 2020). The trends in the maximum SIE are significantly different than zero, and in line with observations in the Medium and High resolution models, but smaller and non significant in the Low resolution model which shows a trend comparable to that of the 1980-1999 observational record (results not shown). Note that the Medium resolution model remains in very good agreement with observations over the satellite era.

After a doubling of CO_2 concentration, none of the three simulations reach an ice-free Arctic (defined as SIE < 1 million km^2; IPCC, 2013). The minima of SIE reached by the CM2-O suite at the end of the CC simulation are generally higher than in the other models participating in CMIP6. Indeed, the majority of climate model simulations reach a sea ice free Arctic in the summer by the year 2050 with a CO_2 concentration ranging between 500 and 550 ppm depending on the emission scenario (Fig.3 and Table S4 of Notz & SIMIP Community, 2020).

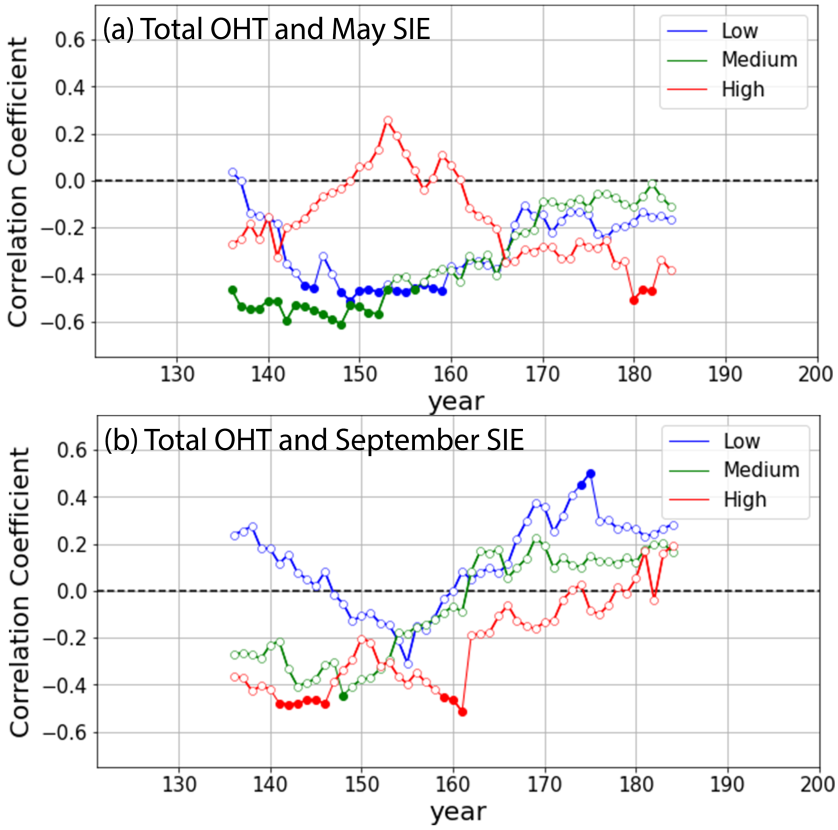

Figure 5. Twenty-year moving window correlation between the detrended annual (January-December) total OHT and the detrended (a) May SIE and (b) September SIE in the CC run. Full circles indicate the 95% confidence level.

We note that the High resolution model loses significantly more sea ice under climate change than the Low resolution models (Figs. 2 and 3 , and Table 1), though both have very similar initial conditions throughout the preindustrial era (not shown). Conversely, the Medium and High resolution models display the same trends under climate change in both seasons despite starting from very different SIE preindustrial conditions (Fig. 3 and Table 1). Hence, the lower SIE at the end of the CC run in the Medium resolution model is mostly due to the preindustrial mean state (low initial sea ice cover), rather than to a strong response to the CO_2 increase.

The OHT is sensitive to the CO_2 increase in all three models, but the intensity of the response varies across the models (Fig. 3 b). By the end of the simulation, the total OHT has increased by $\sim$ 50% in the Medium resolution model while it has doubled in the High and Low resolution models. The response of the Low resolution OHT is weaker than that of the CESM-LE model of the same resolution (Auclair & Tremblay, 2018). In the Medium resolution model, the OHT increase is mostly linear, with a strong decadal variability. In the Low and High resolution models, a significant multi-decadal signal is super imposed on the linear increase in OHT, resulting in two "apparent" stable periods without OHT trends (in the first three decades and last two-three decades) and a relatively rapid increase between the fourth and fifth decades.

In the Medium resolution model, we see a weak signal at decadal time scale in March SIE in the first half of the record, and a stronger decadal signal in September SIE that persists until the end of the simulation (see Fig. 3). We will see in Section 4.3 that this signal is driven mostly by the OHT from the Atlantic driving sea ice loss in the Greenland and Barents Seas. We note that the signal is not as strong as for the High resolution model. Presumably, this is due to the fact that the sea ice cover retreats north of the Barents Sea continental shelf in the middle of the simulation ($\sim$ year 150, i.e. between the third and fourth decade; see Fig. 4), at which point the ocean heat is not in direct contact with the sea ice anymore (Auclair & Tremblay, 2018). Similarly, at an interannual time scale, the total OHT in the Medium resolution model is negatively correlated with the May SIE until $\sim$ year 150, after which the correlation reduces (Fig. 5).

In the Low resolution model, the decadal variability in SIE and OHT are maximum and mimimum (respectively) across the suite (Fig. 3). Hence, the decadal variability in the pan-Arctic SIE is not dominated by OHT variability in that model. We will see in Section 4.3 that the OHT and SIE are linked at regional scale (i.e in the Atlantic and Pacific sectors), but that the two regional signals are out of phase and not apparent in the total SIE and OHT. At the interannual time scale, the total OHT is significantly correlated with May SIE in the Low resolution model from year 143 until year 160, with higher OHT leading to lower SIE. From year 160 onward, no significant correlation is found (Fig. 5).

In the High resolution model, the variability in OHT at decadal time scale is linked with variability in September SIE (correlation coefficient of -0.51 significant at the 95% confidence level; Fig. 3). At interannual time scale, the total OHT is correlated with September SIE until $\sim$ year 160, and with May SIE in the last 20 years of the simulation, although the signal is not robust (i.e. the correlation is only significant for the last few years; Fig. 5). Again, the shift in correlations at year 160 corresponds to a significant retreat of sea ice in the Barents Sea (Fig. 4 and discussion in section 4.3).

The links between the internannual variability in SIE and total OHT in the CM2-O model suite do not persist throughout the CC simulation, and are not always present in the CTRL simulation (not shown). Hence, OHT variability is not the only driver of SIE variability for any of the models. However, all models show correlations between SIE and OHT at decadal or interannual scale at the beginning of the simulation, which corresponds to the period when sea ice cover is larger, especially in the Barents Sea where a strong influence of the ocean on sea ice is expected (Auclair & Tremblay, 2018; Årthun et al., 2012). This suggests that OHT variability is a major driver of sea ice variability at regional scale.

4.3 Impact of OHT on SIE at Regional Scale

4.3.1 Temporal Scales of Correlations between OHT and SIE

In the three main sectors of the Arctic, all models generally show an increase in OHT concurrent with a decrease in SIE in the CC simulation (Fig. 6). There is an exception in the March SIE for the Low resolution model (Atlantic sector) which shows an increase in SIE (years 165-175) despite the increase in OHT, indicating that the natural variability at decadal time scale in this model is larger than the forced change associated with the CO_2 increase. At the multi-decadal time scale, all models show an abrupt increase in OHT in the Barents Sea Opening at the mid-simulation that is concurrent with an abrupt decline in SIE mostly visible in March in the Atlantic (Figs. 6 a-c and 4). The September SIE does not react to the abrupt Barents Sea Opening OHT however, indicative that summer processes (e.g. ice-albedo feedback) have more impact than previous winter preconditioning in the model suite.

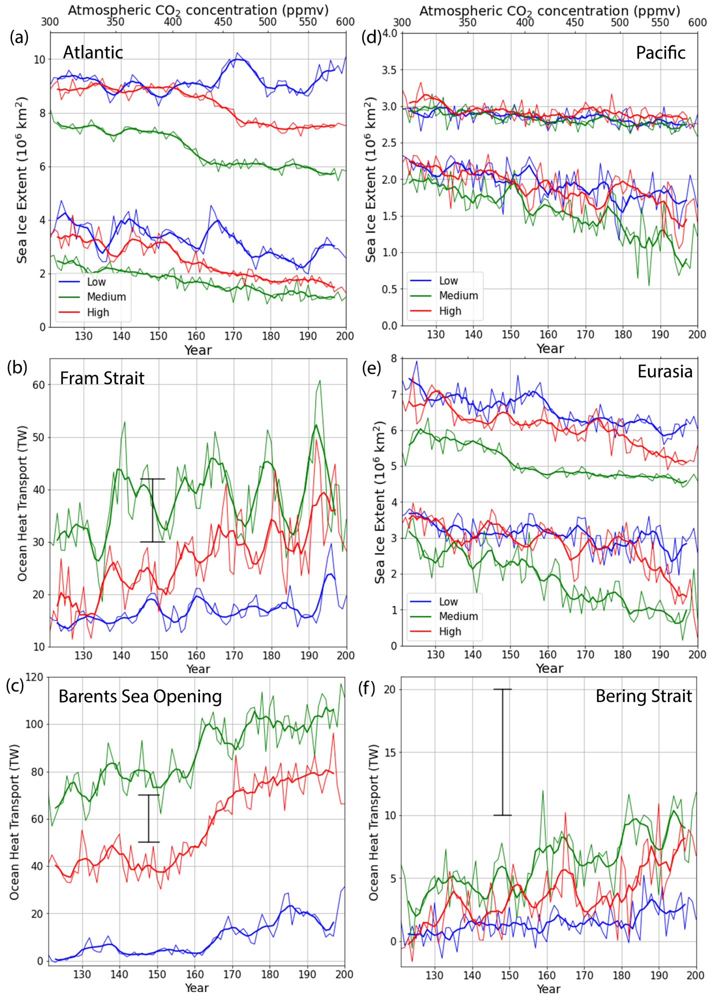

Figure 6. March and September SIE (thin lines) and five year running mean (thick lines) in (a) the Atlantic sector, (b) the Pacific sector and (c) the Eurasian sector, and annual OHT (thin lines) and five year running mean (thick lines) through (b) the Fram Strait, (c) the Barents Sea Opening and (f) the Bering Strait in the CC run for the Low, Medium and High resolution models as a function of time (top axis) and CO_2 concentration (bottom axis). Observational estimates are indicated as vertical bars with the horizontal extent corresponding to the period of observation: (b) 1997-2009 (Schauer & Beszczynska-Moeller, 2009), (c) 1997-2007 (Smedsrud et al., 2010), and (f) 1998-2007 (Woodgate et al., 2010).

In the Medium resolution model, the Fram Strait OHT increases in the second decade by about 15 TW, which is concurrent with a very slight local minimum in SIE. The Fram Strait OHT sees another sharp increase of 10 TW in the fourth decade, which is followed by an abrupt increase of 20 TW in the Barents Sea Opening in the fifth decade. Those increases match a sudden decrease in March SIE in the Atlantic sector that is sustained until the end of the simulation (Fig. 6 a-c). The Bering Strait OHT increases throughout the simulation, with a sharper increase in the fourth decade that also matches significant sea ice loss in the Eurasian sector (Figs. 4 b and 6 e-f). By the end of the simulation, the OHT in the Bering Strait reaches the lower range of current observations (10 TW).

In the High resolution model, the OHT remains fairly constant in the Barents Sea Opening until the fourth decade (equivalent CO_2 concentration around 400 ppmv) when an OHT increase of 30 TW occurs, after which the OHT stabilizes again until the end of the simulation (Fig. 6 c). These changes match well the pattern of sea ice melt in the Atlantic Sector in both March and September (Figs. 4 c and 6 a). We note that while the September sea ice loss is concurrent with the Barents Sea Opening OHT increase in the High resolution model, the March sea ice loss is delayed by $\sim$ 10 years. In the Atlantic sector, the decadal variability in the September SIE appears to be mostly driven by Fram Strait variability in the first half of the simulation. This is unexpected, given that Atlantic Water masses are located at 100 m depth in the Fram Strait (not shown). The decadal variability in the Bering Strait OHT also matches well the decadal variability in September SIE in the Eurasian Sector, as a sharp increase in Bering Strait OHT in the last 25 years of the simulation is concurrent with a decline in March and September SIE in the Eurasian sector (Fig. 6 e-f).

In the Low resolution model, the significant increase in Barents Sea Opening OHT happens around the fourth decade when the OHT goes from near zero to about 20 TW by the end of the simulation. This increase in OHT is concurrent with the retreat of sea ice in the Barents Sea after the fourth decade (Figs. 4 a and 6 a and c). The decadal variability in the Fram Strait OHT is well correlated with decadal variability in the Atlantic sector September SIE during the first half of the simulation. In the Eurasian sector, the decrease in SIE at the end of the simulation is concurrent with an OHT increase in the Bering Strait.

4.3.2 Spatial Patterns of Correlations between OHT and SIE

We now turn to spatial correlations between OHT and Sea Ice Concentration (SIC) anomalies to unravel some major modes of variability at the Pan-Arctic scale and the impact of OHT on sea ice decline at the regional scale.

A dipole between the Atlantic and the Pacific sectors appear in all models with the Bering Strait OHT and SIC anomalies having opposite sign correlations in the Pacific/Eurasian sectors and the Atlantic sector (Fig. 7 a-c). This is in accord with results from the CESM-LE (Auclair & Tremblay, 2018), and follows from the fact that, to first order, the volume of water in the Arctic is conserved, hence there is a compensation of ocean volume transport (OVT) between the two sectors (Timmermans & Marshall, 2020). In the Medium and High resolution models, we also find a consistent dipole with opposite sign correlations between SIC variability in the Barents/Greenland seas, and the Labrador Sea. This is a standard signal in the observational record linked with the North Atlantic Oscillation (NAO) variability (Venegas & Mysak, 2000). In the Medium resolution model, the correlations are weaker in the Barents Sea Opening because the sea ice edge is retreated northward compared to the Low and High resolution models (see Fig. 2, 4).

In the Medium resolution model, the most significant correlations stem from OHT in the Bering and Fram Straits. The Bering Strait OHT is correlated negatively with most of the Pacific side of the Arctic, even well into the Kara Sea, and is positively correlated with SIC in the Barents Sea and Greenland Sea (Fig. 7 b). This is in accord with the three major pathways of Pacific Waters into the Arctic : the Alaskan current branch, the branch that spills over the Chukchi shelf and enters the Canada/Makarov Basin, and the branch that stays on the Eurasian shelf (Pickart, 2004; Yamamoto-Kawai et al., 2008).

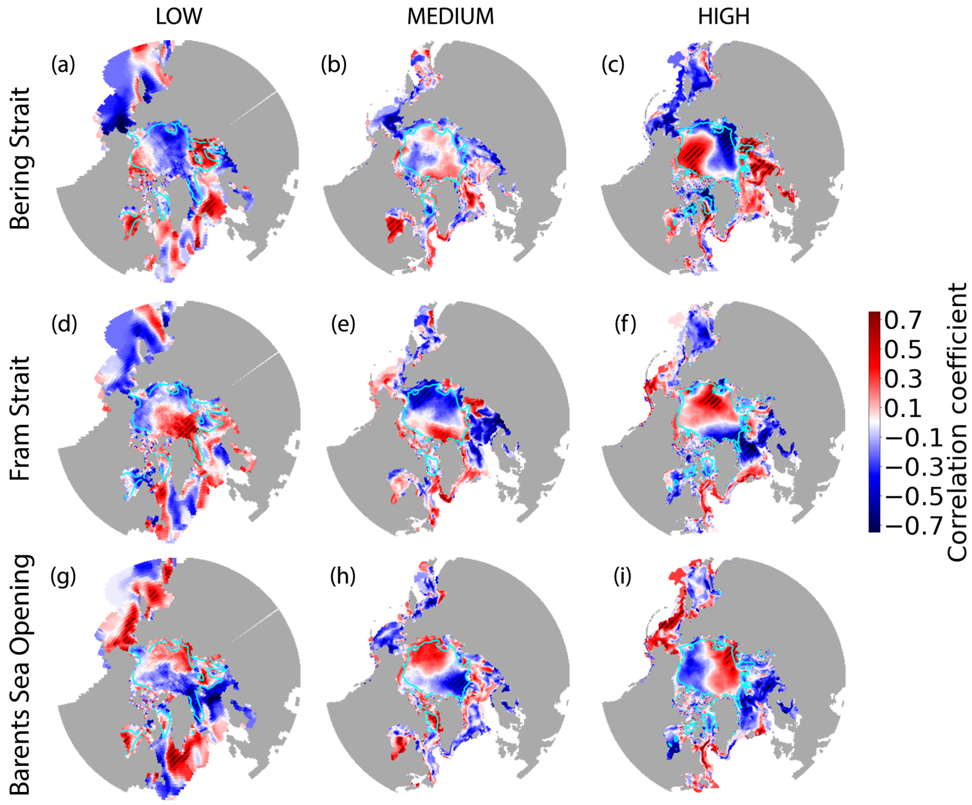

Figure 7. Correlation maps between the detrended annual (January-December) OHT in the Bering Strait (a-c), Fram Strait (d-f) and Barents Sea Opening (g-i) and the detrended May sea ice concentration (SIC), in the Low (left), Medium (center) and High (right) resolution models in the CC experiments. Inside the blue contour lines are areas where the SIC varies by less than 5%. The dashed areas is the 95% significance level.

The Fram Strait OHT is strongly linked with sea ice melt in the Greenland Sea, Barents Sea and even in the Chuchki Sea (Fig. 7 e). The Barents Sea Opening OHT is not significantly correlated with sea ice loss anywhere in the Arctic, although a weak but widespread negative correlation pattern appears in the Barents Sea and in the Eurasian Basin (Fig. 7 h). OHTs across the three main gates are shown to be mostly positively correlated with SIC into the Baffin Bay, Hudson Bay and Labrador Sea, which reflects a partitioning of the heat transport between the Arctic and the Irminger current, associated with the NAO variability Straneo and Heimbach (2013) as we will see in section 5.

In the Low resolution model, we see a significant negative correlation between Bering Strait OHT and SIC in the East Siberian sector (Fig. 7 a). In this model, the branch of Pacific Waters that stays on the Eurasian shelf is dominant for the sea ice variability, in accord with the CESM-LE (Auclair & Tremblay, 2018). The Fram Strait OHT is significantly correlated to sea ice loss in the Greenland Sea and the Labrador Sea, as well as on the Barents Sea Shelf, but positively correlated with SIC around the Fram Strait itself (Fig. 7 d). Finally, the Barents Sea Opening OHT is strongly correlated with sea ice loss both in the Barents Sea and the Fram Strait (Fig. 7 g). Again, conservation of mass dictates more outflow of cold and fresh waters in the western Fram Strait when more inflow of Atlantic Water is present.

In the High resolution model, the Bering Strait OHT is negatively correlated with SIC in the Bering Sea and Chuchki Sea, as well as the Baffin Bay. For both Fram Strait and Barents Sea Opening OHT, the negative correlations with SIC are significant in the Greenland Sea, the Fram Strait and the Barents Sea ans Kara Sea (Fig. 7 f,i). We also note that Fram Strait and Barents Sea Opening OHTs are positively correlated with SIC in the Baffin Bay and Labrador sea, although the correlations are less significant (again, this is the typical dipole in SIC in the Barents and Labrador Seas).

This analysis reveals more robust coupling between OHT and SIE at the regional scale, especially in the Atlantic sector where Atlantic sea ice loss is driven by OHT increase, in particular in the Barents Sea as shown in Figure 4. Significant correlations at interannual and decadal time scales are exhibited between Bering Strait OHT and SIE in the Eurasian Sector, and between the Fram Strait and Barents Sea Opening OHT in the Greenland and Barents Seas.

5 Discussion

Of the three models, the Medium resolution model has the largest OHT into the Arctic and smallest winter and summer SIE, both of which are in good agreement with observations. The correct seasonal cycle in SIE is achieved at the expense of a low bias in sea ice thickness. We find that in the CM2-O suite, the OHT increases with increasing resolution from the Low to the Medium resolution model, in agreement with results from Docquier et al. (2019), but decreases as the resolution increases further from the Medium to the High resolution model, in contrast with Docquier et al. (2019). Note that the increase in OHT in response to the CO_2 increase is slightly larger in the High resolution model than in the Medium resolution model, so that the higher OHT and lower SIE in the Medium resolution model at the end of the CC simulation are primarily due to the preindustrial mean state. The High resolution model OHT is larger than that of the Low resolution model, yet the mean sea ice states in the preindustrial and early CC simulations are similar. This is in contrast with the study by Kirtman et al. (2012) who also find a larger OHT when increasing the resolution in their analysis of the NCAR Community Climate System Model version 3.5 (CCSM3.5) from 1° to 1/10° but a smaller sea ice extent in the High resolution model. The low OHT in the NCAR Low resolution model is mostly attributed to the poor representation of the Norwegian Coastal Current in the model, in accord with results from the CM2-O Low resolution model (Fig. 8 g). The decrease in OHT from the Medium resolution to the High resolution is also in contrast with the results from Hewitt et al. (2016) though the resolution of the atmosphere and the frequency of the ocean/atmosphere coupling is also increased between their two model versions. We note that OHT and SIE correlations are not sensitive to an increase in spatial resolution of the atmosphere component (Docquier et al., 2019). The stronger OHT in our Medium resolution model occurs despite a weaker AMOC (not shown), in contrast with results by Jackson et al. (2020). This suggests that the higher OHT in the Medium resolution model is linked with the surface ocean circulation (gyre transport) rather than the meridional circulation (Griffies et al., 2015). We argue that differences in current pathways could explain the changes in Arctic OHT in the models.

All three models agree broadly in the structure of the currents in northern North Atlantic (Fig. 8 g-i). The Low resolution model however has broader and significantly weaker currents than the Medium and High resolution models over the Arctic. The most striking difference with the other two models is the absence of the West Greenland Current and Labrador Sea current at the surface (Fig. 8 g). In the Low resolution model, Atlantic Waters enter the Labrador Sea and Baffin Bay at depth (Fig. 8 a, d) and fresh cold Arctic Waters - entering from Lancaster Sound and the Nares Strait - flow southward at the surface. The same top/bottom structure of ocean current is present in the Fram Strait, where Arctic Waters flow southward along the East Greenland coastline and Atlantic Waters flow northward at depth (West Spitsbergen current; results not shown).

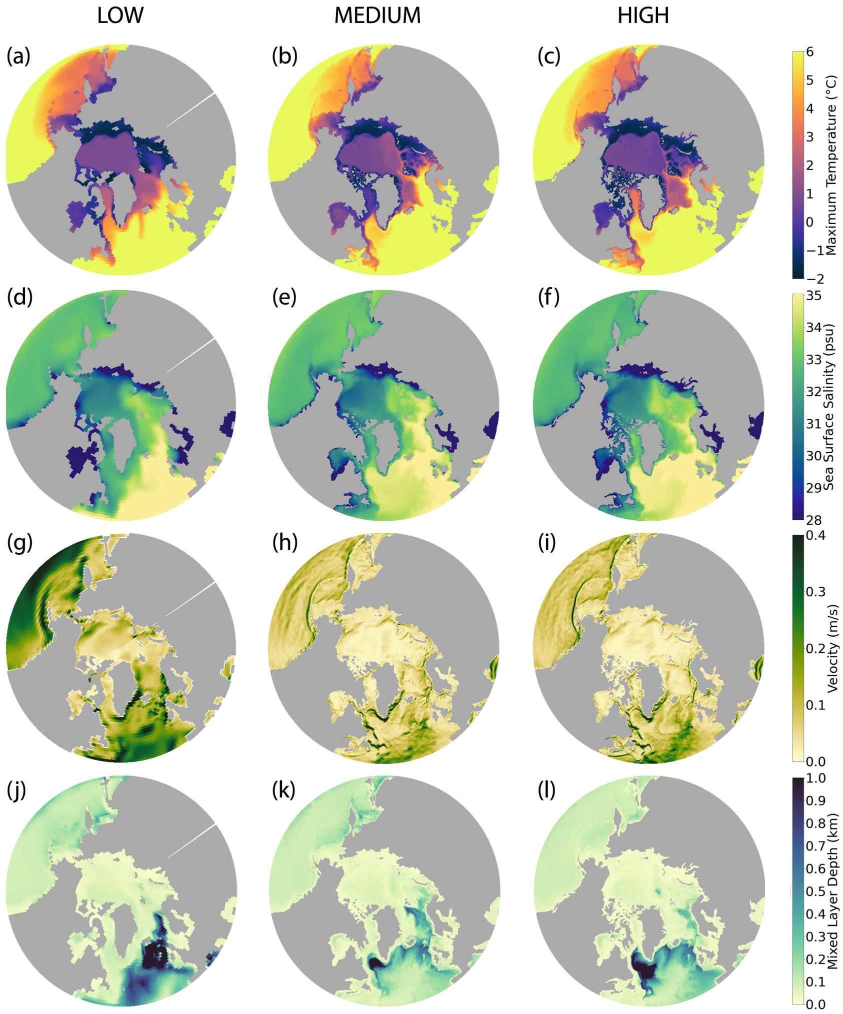

Figure 8. Mean temperature maximum (a-c), sea surface salinity (d-f), surface velocities (g-i) and winter mixed layer depth (h-l) averaged over the first decade (years 120-129) of the CC experiment for the Low (left column), Medium (middle column) and High (right column) resolution models. Note that the colorbars are always the same between the models, except for figure (g) where the Low resolution velocity is multiplied by a factor 4 to highlight the pathways of currents.

In the High resolution model, Atlantic Waters penetrate far north into the Baffin Bay. The Medium resolution model contrasts with the other two models in the Baffin Bay, where very little Atlantic Water enters (Figs. 8 b and 9). Instead, Atlantic Waters flow cyclonically around the Labrador Sea along the continental shelf (Fig. 8 h).

The path of the Atlantic Waters and penetration of heat into the Baffin Bay is known to be influenced by the atmospheric forcing (D. Holland et al., 2008). In particular, the partitioning of OHT between the North Atlantic Drift and the Irminger Current (south of Iceland) is sensitive to the state of the NAO, with positive phase of the NAO favoring the eastern branch of the circulation, which is then associated with a reduced ice cover in the Greenland and Barents Seas (Myers et al., 2007; Strong et al., 2009; Straneo &

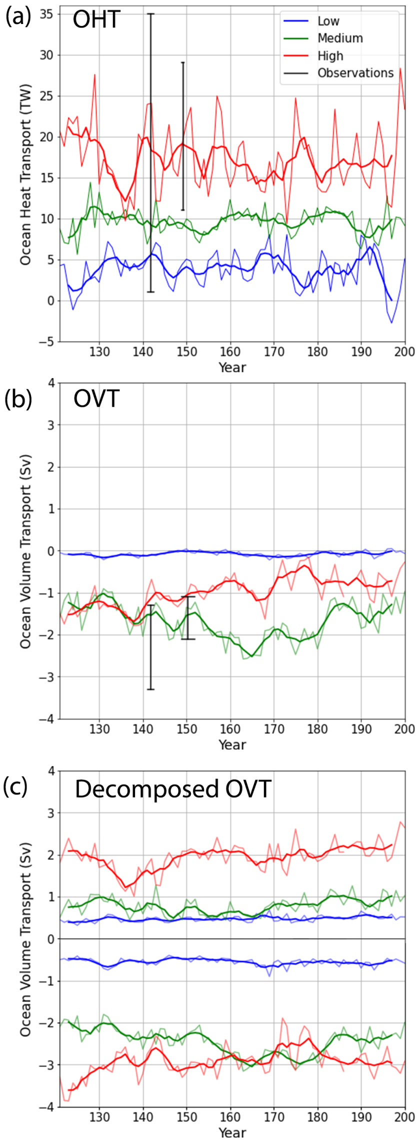

Figure 9. Timeseries of (a) total OHT and (b) total OVT across Davis Strait in the CC run for the Low, Medium and High resolution models. The total OVT is decomposed into its northward (positive) and southward (negative) component in (c). Thin lines correspond to annual averages and thick lines to five-year running mean. Observational estimates are indicated as vertical bars with the horizontal extent corresponding to the period of observations: 1987-1990 (Cuny et al., 2004) and 2004-2005 (Curry et al., 2011) for OHT, 1987–1990 (Cuny et al., 2004) and 2004-2010 (Curry et al., 2014) for OVT.

.

Heimbach, 2013). In climate models, the NAO has been shown to influence Labrador Sea Water formation on decadal time scales, which in turn affects the subpolar gyre (Langehaug et al., 2012). During the spin up of our models (years 1 to 120), the mean state of the atmosphere changes to a more positive NAO state in the Low and High resolution models compared to the Medium resolution model (not shown). This state persists throughout the CC simulation (see Fig. 10), and should promote deeper penetration of Atlantic

Waters in the Fram Strait and Barents Sea Opening in the Low and High resolution models (Langehaug et al., 2012). Instead, we see more recirculation of Atlantic Waters in the Irminger Sea in the High resolution model compared to the Medium resolution model, indicating the NAO variability is not the leading factor in determining the current pathways in the Arctic.

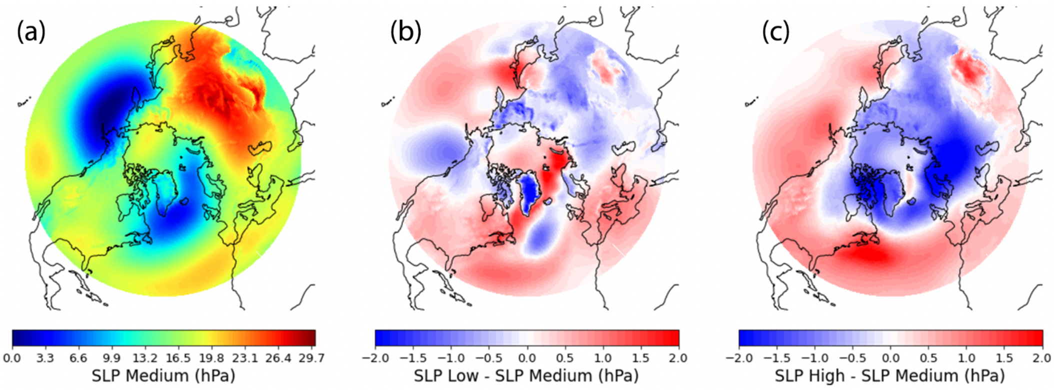

Figure 10. Winter SLP (JFM) in the Medium resolution model (a), winter SLP difference between the Low and Medium resolution models (b) and winter SLP difference between the High and Medium resolution models (c) averaged over the CC simulation

The path of warmer Atlantic Waters into the Baffin Bay is also sensitive to spatial resolution in models, with high resolutions (up to 1/60°) favoring the Irminger branch (Pennelly & Myers, 2020). Although all three models fall within the range of observations for OHT through the Davis Strait, the High resolution model is the closest to the mean and has the largest interannual and decadal variability of the suite, yet still smaller than observations (Fig. 9). Importantly, the OHT accross the Davis Strait in the High resolution model is the highest across the suite, about twice as large as the OHT in the Medium resolution model, and four times that of the Low resolution (Fig. 9 a). The OVT in the Medium and High resolution models remain close to observations, but is much weaker in the Low resolution model (Fig. 9 b). Very little poleward volume transport is found in the Medium and Low resolution models compared to the High resolution model, and the Medium and High resolution models have very similar southward volume transports (Fig. 9 c). The lack of poleward transport is in agreement with the representation of currents in the Medium and Low resolution models, where the branch going into the Baffin Bay is not as strong as in the High resolution model (Fig. 8 g-i). The interannual variability of OVT in Davis Strait is significantly anti-correlated (at the 95% confidence level) with the sum of the transport through the Fram Strait and Barents Sea Opening, with correlation coefficients of -0.82, -0.96 and -0.82 in the Low, Medium and High resolution models, respectively. This suggests that the Irminger Branch dominates the variability in the Davis Strait as opposed to the East Greenland Current branch bringing polar surface waters southward. This anticorrelation also illustrates the partitioning of the transport of Atlantic Waters between the Arctic and the Labrador Sea and Davis Strait. Hence, in the Medium resolution model, the weaker OVT into the Davis Strait is tied to the higher OHT into the Arctic through the Fram Strait and Barents Sea Opening.

In the model suite, the difference in the partitioning of Atlantic waters between the Irminger branch and Norwegian branch can be partly related to the difference in convection centers. In the Medium resolution model, mixed layer in the Labrador Sea is slightly deeper but more localized than in the High resolution model (Fig. 8 j-l). The maximum winter mixed layer depth (MLD) in the Medium resolution model is 1.7 km in the first decade of the CC run, around 300 m deeper than in the High resolution model. The area of deep convection in the High resolution model extends to the western boundary of the Labrador Sea, with MLD of around 1 km. Similarly in the HighResMIP models, 1/4° models show deeper convection than 1° models, and overestimate MLD compared to observations (Koenigk et al., 2021). Pennelly and Myers (2020) also find that increasing the ocean resolution from 1/4° to 1/12° (and even 1/60°) leads to a shallower mixed layer thanks to more representation of eddy fluxes; however, they also find that the area of deep convection is less extensive. Conversely, in the Icelandic and Norwegian Seas, the depth and area of deep mixed layer are greater in the Medium resolution model than in the High resolution model. From Low to High resolutions, we see a south-westward transfer of deep convection regions from the Greenland-Icelandic-Norwegian (GIN) Seas towards the Labrador Sea (see Fig. 8 j-l).

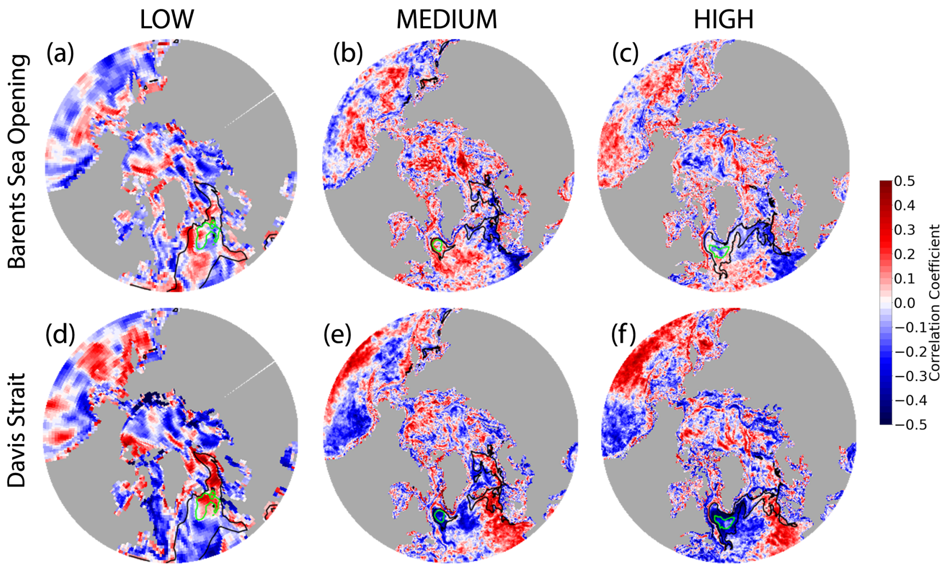

Figure 11. Correlation maps between the detrended annual (January-December) OVT in the Barents Sea Opening (a-c) and Davis Strait (d-f) and the detrended Winter MLD, in the Low (left), Medium (center) and High (right) resolution models in the CC experiments. Black contours indicate the CC simulation average winter MLD at 300 m (black line) and 1 km (green line).

In the northern North Atlantic, where deep convection is present, we find a strong negative correlation at interannual scale between the OVT across the Barents Sea Opening and winter MLD in both the Medium and High resolution models (Figs. 11 b-c and 8 h-l), indicating that deep penetration of Atlantic Waters into the Barents Sea Opening is associated with weak convection in the GIN Seas. Similarly, the OVT across Davis Strait is negatively correlated with winter MLD in the Labrador Sea in all three models (Fig. 11), indicating that deep penetration of Atlantic Waters into Baffin Bay through the Davis Strait is associated with weak convection in the Labrador Sea. This negative correlation suggests that a weak subpolar gyre circulation is associated with strong deep convection and meridional circulation, in agreement with results from Drijfhout and Hazeleger (2006).

6 Conclusion

In this study, we investigated the impact of ocean heat transport on Arctic sea ice under climate change in the GFDL CM2-O model suite. The models of the suite only differ in their ocean horizontal spatial resolution : from 1° (Low) to 0.25° (Medium) to 0.1° (High), with a mesoscale eddy parameterization for the Low resolution model. We investigated the potential impact of resolution on the mean ocean and sea ice states, and the relationship between Arctic ocean heat transport and sea ice, on the Pan-Arctic and regional scale, at annual and decadal time scales. We found that :

- Models with a higher total ocean heat transport into the Arctic have a smaller sea ice extent in all seasons.
- Decadal variability in ocean heat transport explains a large fraction of decadal variability in sea ice extent.
- At interannual time scale, the impact of ocean heat transport on sea ice extent is limited to the shelf regions.
- The Medium resolution model is in best agreement with the observational record at the beginning of the satellite era.
- The Medium resolution model has the highest ocean heat transport into the Arctic and lowest sea ice extent in the suite of models both in the pre-industrial and climate change runs, in contrast with the conclusions from Docquier et al. (2019) who state that higher resolution models result in more ocean heat transport in the Arctic. We note that our results are in agreement with Docquier et al. (2019) for a narrower range of spatial resolution similar to theirs (low to medium resolutions).
- Though the Medium resolution has a higher ocean heat transport and lower sea ice extent when compared with those of the High resolution model in the pre-industrial mean state, the trends in sea ice loss and ocean heat transport in the two models under increasing CO_2 forcing are similar.
- The Low and High resolution models have the same pre-industrial sea ice extent and thickness distribution, but very different response in sea ice extent to CO_2 forcing, with the High resolution model being more sensitive than its coarser resolution counterpart.
- As the spatial resolution of the model increases from medium to high, greater heat transport is found into Davis Strait at the expense of the Atlantic-Arctic gates suggesting that the Irminger branch is favored over the Faroe-Scotland branch. The differences in deep convection between these two models might partly explain the difference in heat partitioning.

Acknowledgments

M.D. acknowledges support from the Fonds de recherche du Québec Nature et technologies (FRQNT) through the Bourse de maîtrise en recherche. M.D. and C.O.D. acknowledge the support of the Natural Sciences and Engineering Research Council of Canada (NSERC) - Accelerator program. M.D. is also grateful for the support of McGill University, Québec-Océan and Arctrain Canada. This work is a contribution to the NSERC - Discovery Program, Marine Environmental Observation, Prediction and Response (MEOPAR), NASA grant #80NSSC20K1259, NSF – Office of Polar Program grants #1504023, #1603350 and #1928126, awarded to BT.

All output variables from the the NSIDC are available at https://nsidc.org/data/G02135/versions/3 for monthly sea ice extent and https://nsidc.org/data/G10010 for the SIBT1850 data. Output of the GFDL CM2-O suite that were used to make the figures of the paper will be available from the Polar Data Catalogue (https://www.polardata.ca/) by acceptance.

References

Anderson, J. L., Balaji, V., Broccoli, A. J., Cooke, W. F., Delworth, T. L., Dixon, K. W., ... Wyman, B. L. (2004). The new gfdl global atmosphere and land model am2-lm2: Evaluation with prescribed sst simulations [Journal Article]. *Journal of Climate*, *17*(24), 4641-4673. Retrieved from http://pubs.er.usgs.gov/publication/70026156

Årthun, M., Eldevik, T., & Smedsrud, L. H. (2019). The role of atlantic heat transport in future arctic winter sea ice loss [Journal Article]. *Journal of Climate*, *32*(11), 3327-3341. doi: 10.1175/JCLI-D-18-0750.1

Årthun, M., Eldevik, T., Smedsrud, L. H., Skagseth, Ø., & Ingvaldsen, R. B. (2012). Quantifying the influence of atlantic heat on barents sea ice variability and retreat [Journal Article]. *Journal of Climate*, *25*(13), 4736-4743. Retrieved from https://journals.ametsoc.org/view/journals/clim/25/13/jcli-d-11-00466.1.xml doi: 10.1175/jcli-d-11-00466.1

Auclair, G., & Tremblay, L. B. (2018). The role of ocean heat transport in rapid sea ice declines in the community earth system model large ensemble [Journal Article]. *Journal of Geophysical Research: Oceans*, *123*(12), 8941-8957. Retrieved from https://agupubs.onlinelibrary.wiley.com/doi/abs/10.1029/2018JC014525 doi: 10.1029/2018jc014525

Barton, B. I., Lenn, Y., & Lique, C. (2018). Observed atlantification of the barents sea causes the polar front to limit the expansion of winter sea ice [Journal Article]. *Journal of Physical Oceanography*, *48*(8), 1849-1866. doi: 10.1175/JPO-D-18-0003.1

Beszczynska-Möller, A., Woodgate, R., Lee, C., Melling, H., & Karcher, M. (2011). A synthesis of exchanges through the main oceanic gateways to the arctic ocean [Journal Article]. *Oceanography (Washington D.C.)*, *24*. doi: 10.5670/oceanog.2011.59

Bitz, C. M., Fyfe, J., & Flato, G. (2002, 03). Sea ice response to wind forcing from amip models. *Journal of Climate - J CLIMATE*, *15*, 522-536. doi: 10.1175/1520-0442(2002)015⟨0522:SIRTWF⟩2.0.CO;2

Bitz, C. M., Holland, M. M., Hunke, E. C., & Moritz, R. E. (2005). Maintenance of the sea-ice edge [Journal Article]. *Journal of Climate*, *18*(15), 2903-2921. Retrieved from https://doi.org/10.1175/JCLI3428.1 doi: 10.1175/JCLI3428.1

Bitz, C. M., Holland, M. M., Weaver, A. J., & Eby, M. (2001). Simulating the ice-thickness distribution in a coupled climate model [Journal Article]. *Journal of Geophysical Research: Oceans*, *106*(C2), 2441-2463. Retrieved from https://agupubs.onlinelibrary.wiley.com/doi/abs/10.1029/1999JC000113 doi: https://doi.org/10.1029/1999JC000113

Bitz, C. M., & Lipscomb, W. H. (1999). An energy-conserving thermodynamic model of sea ice [Journal Article]. *Journal of Geophysical Research: Oceans*, *104*(C7), 15669-15677. Retrieved from https://doi.org/10.1029/1999JC900100 doi: https://doi.org/10.1029/1999JC900100

Bitz, C. M., & Roe, G. H. (2004). A mechanism for the high rate of sea ice thinning in the arctic ocean [Journal Article]. *Journal of Climate*, *17*(18), 3623-3632. Retrieved from https://doi.org/10.1175/1520-0442(2004)017<3623:AMFTHR>2.0.CO;2 doi: 10.1175/1520-0442(2004)017⟨3623:AMFTHR⟩2.0.CO;2

Bourke, R. H., & Garrett, R. P. (1987). Sea ice thickness distribution in the arctic ocean. *Cold Regions Science and Technology*, *13*(3), 259-280. Retrieved from https://www.sciencedirect.com/science/article/pii/0165232X87900073 doi: https://doi.org/10.1016/0165-232X(87)90007-3

Brankart, J.-M. (2013). Impact of uncertainties in the horizontal density gradient upon low resolution global ocean modelling [Journal Article]. *Ocean Modelling*, *66*, 64-76. Retrieved from https://www.sciencedirect.com/

science/article/pii/S1463500313000309 doi: https://doi.org/10.1016/j.ocemod.2013.02.004

Cuny, J., Rhines, P., & Kwok, R. (2004, 01). Davis strait volume, freshwater and heat fluxes [Journal Article]. *Deep Sea Research Part I: Oceanographic Research Papers*, *52*, 519-542. doi: 10.1016/j.dsr.2004.10.006

Curry, B., Lee, C. M., & Petrie, B. (2011). Volume, freshwater, and heat fluxes through davis strait [Journal Article]. *Journal of Physical Oceanography*, *41*(3), 429-436. Retrieved from https://doi.org/10.1175/2010JPO4536.1 doi: 10.1175/2010JPO4536.1

Curry, B., Lee, C. M., Petrie, B., Moritz, R. E., & Kwok, R. (2014). Multiyear volume, liquid freshwater, and sea ice transports through davis strait [Journal Article]. *Journal of Physical Oceanography*, *44*(4), 1244-1266. Retrieved from https://doi.org/10.1175/JPO-D-13-0177.1 doi: 10.1175/JPO-D-13-0177.1

Delworth, T. L., Broccoli, A. J., Rosati, A., Stouffer, R. J., Balaji, V., Beesley, J. A., … Zhang, R. (2006). Gfdl's cm2 global coupled climate models. part i: Formulation and simulation characteristics [Journal Article]. *Journal of Climate*, *19*(5), 643-674. Retrieved from https://journals.ametsoc.org/view/journals/clim/19/5/jcli3629.1.xml doi: 10.1175/jcli3629.1

Delworth, T. L., Rosati, A., Anderson, W., Adcroft, A. J., Balaji, V., Benson, R., … Zhang, R. (2012). Simulated climate and climate change in the gfdl cm2.5 high-resolution coupled climate model [Journal Article]. *Journal of Climate*, *25*(8), 2755-2781. Retrieved from https://doi.org/10.1175/JCLI-D-11-00316.1 doi: 10.1175/jcli-d-11-00316.1

Desmarais, A., & Tremblay, L. B. (2021). Assessment of decadal variability in sea ice in the community earth system model against a long-term regional observational record: Implications for the predictability of an ice-free arctic [Journal Article]. *Journal of Climate*, *34*(13), 5367-5384. Retrieved from https://journals-ametsoc-org.proxy3.library.mcgill.ca/view/journals/clim/34/13/JCLI-D-20-0561.1.xml doi: 10.1175/JCLI-D-20-0561.1

DeWeaver, E., & Bitz, C. M. (2006). Atmospheric circulation and its effect on arctic sea ice in ccsm3 simulations at medium and high resolution [Journal Article]. *Journal of Climate*, *19*(11), 2415-2436. Retrieved from https://doi.org/10.1175/JCLI3753.1 doi: doi.org/10.1175/JCLI3753.1

Docquier, D., Grist, J. P., Roberts, M. J., Roberts, C. D., Semmler, T., Ponsoni, L., … Fichefet, T. (2019). Impact of model resolution on arctic sea ice and north atlantic ocean heat transport [Journal Article]. *Climate Dynamics*, *53*(7), 4989-5017. Retrieved from https://doi.org/10.1007/s00382-019-04840-y doi: 10.1007/s00382-019-04840-y

Drake, H. F., Morrison, A. K., Griffies, S. M., Sarmiento, J. L., Weijer, W., & Gray, A. R. (2018). Lagrangian timescales of southern ocean upwelling in a hierarchy of model resolutions [Journal Article]. *Geophysical Research Letters*, *45*(2), 891-898. Retrieved from https://agupubs.onlinelibrary.wiley.com/doi/abs/10.1002/2017GL076045 doi: https://doi.org/10.1002/2017GL076045

Drijfhout, S. S., & Hazeleger, W. (2006). Changes in moc and gyre-induced atlantic ocean heat transport. *Geophysical Research Letters*, *33*(7). Retrieved from https://agupubs.onlinelibrary.wiley.com/doi/abs/10.1029/2006GL025807 doi: https://doi.org/10.1029/2006GL025807

Drinkwater, K. F., Miles, M., Medhaug, I., Otterå, O. H., Kristiansen, T., Sundby, S., & Gao, Y. (2014). The atlantic multidecadal oscillation: Its manifestations and impacts with special emphasis on the atlantic region north of 60°n [Journal Article]. *Journal of Marine Systems*, *133*, 117-130. Retrieved from https://www.sciencedirect.com/science/article/pii/S0924796313002236 doi: https://doi.org/10.1016/j.jmarsys.2013.11.001

Dufour, C. O., Morrison, A. K., Griffies, S. M., Frenger, I., Zanowski, H., & Winton,

M. (2017). Preconditioning of the weddell sea polynya by the ocean mesoscale and dense water overflows [Journal Article]. *Journal of Climate*, *30*(19), 7719-7737. Retrieved from https://journals.ametsoc.org/view/journals/clim/30/19/jcli-d-16-0586.1.xml doi: 10.1175/jcli-d-16-0586.1

Dunne, J. P., John, J. G., Adcroft, A. J., Griffies, S. M., Hallberg, R. W., Shevliakova, E., ... Zadeh, N. (2012). Gfdl's esm2 global coupled climate–carbon earth system models. part i: Physical formulation and baseline simulation characteristics [Journal Article]. *Journal of Climate*, *25*(19), 6646-6665. Retrieved from https://doi.org/10.1175/JCLI-D-11-00560.1 doi: 10.1175/jcli-d-11-00560.1

Ferrari, R., Griffies, S. M., Nurser, A. J. G., & Vallis, G. K. (2010). A boundary-value problem for the parameterized mesoscale eddy transport [Journal Article]. *Ocean Modelling*, *32*(3), 143-156. Retrieved from https://www.sciencedirect.com/science/article/pii/S1463500310000065 doi: https://doi.org/10.1016/j.ocemod.2010.01.004

Fetterer, F., Knowles, K., Meier, W. N., Savoie, M., & Windnagel, A. K. (2017). *Sea ice index, version 3.* (Boulder, Colorado USA. NSIDC: National Snow and Ice Data Center. Data accessed 01/2020) doi: 10.7265/N5K072F8

Flato, G. M. (2011). Earth system models: an overview [Journal Article]. *WIREs Climate Change*, *2*(6), 783-800. Retrieved from https://doi.org/10.1002/wcc.148 doi: https://doi.org/10.1002/wcc.148

Fox-Kemper, B., Danabasoglu, G., Ferrari, R., Griffies, S. M., Hallberg, R. W., Holland, M. M., ... Samuels, B. L. (2011). Parameterization of mixed layer eddies. iii: Implementation and impact in global ocean climate simulations [Journal Article]. *Ocean Modelling*, *39*(1), 61-78. Retrieved from https://www.sciencedirect.com/science/article/pii/S1463500310001290 doi: https://doi.org/10.1016/j.ocemod.2010.09.002

García-Quintana, Y., Courtois, P., Hu, X., Pennelly, C., Kieke, D., & Myers, P. (2019). Sensitivity of labrador sea water formation to changes in model resolution, atmospheric forcing, and freshwater input [Journal Article]. *Journal of Geophysical Research: Oceans*, *124*. doi: 10.1029/2018JC014459

Gent, P. R., Willebrand, J., McDougall, T. J., & McWilliams, J. C. (1995). Parameterizing eddy-induced tracer transports in ocean circulation models [Journal Article]. *Journal of Physical Oceanography*, *25*(4), 463-474. Retrieved from https://journals.ametsoc.org/view/journals/phoc/25/4/1520-0485_1995_025_0463_peitti_2_0_co_2.xml doi: 10.1175/1520-0485(1995)025⟨0463:peitti⟩2.0.co;2

Griffies, S. M., Winton, M., Anderson, W. G., Benson, R., Delworth, T. L., Dufour, C. O., ... Zhang, R. (2015). Impacts on ocean heat from transient mesoscale eddies in a hierarchy of climate models [Journal Article]. *Journal of Climate*, *28*(3), 952-977. Retrieved from https://doi.org/10.1175/JCLI-D-14-00353.1 doi: 10.1175/jcli-d-14-00353.1

Grist, J. P., Josey, S. A., New, A. L., Roberts, M., Koenigk, T., & Iovino, D. (2018). Increasing atlantic ocean heat transport in the latest generation coupled ocean-atmosphere models: The role of air-sea interaction [Journal Article]. *Journal of Geophysical Research: Oceans*, *123*(11), 8624-8637. Retrieved from https://agupubs.onlinelibrary.wiley.com/doi/abs/10.1029/2018JC014387 doi: https://doi.org/10.1029/2018JC014387

Haarsma, R. J., Roberts, M. J., Vidale, P. L., Senior, C. A., Bellucci, A., Bao, Q., ... von Storch, J.-S. (2016). High resolution model intercomparison project (highresmip v1.0) for cmip6. *Geoscientific Model Development*, *9*(11), 4185–4208. Retrieved from https://gmd.copernicus.org/articles/9/4185/2016/ doi: 10.5194/gmd-9-4185-2016

Hallberg, R. (2013). Using a resolution function to regulate parameterizations of oceanic mesoscale eddy effects [Journal Article]. *Ocean Modelling*, *72*, 92-103.

Retrieved from https://www.sciencedirect.com/science/article/pii/S1463500313001601 doi: https://doi.org/10.1016/j.ocemod.2013.08.007

Hewitt, H. T., Roberts, M. J., Hyder, P., Graham, T., Rae, J., Belcher, S. E., ... Wood, R. A. (2016). The impact of resolving the rossby radius at mid-latitudes in the ocean: results from a high-resolution version of the met office gc2 coupled model [Journal Article]. *Geoscientific Model Development*, *9*(10), 3655–3670. Retrieved from https://gmd.copernicus.org/articles/9/3655/2016/ doi: 10.5194/gmd-9-3655-2016

Holland, D., Thomas, R., Deyoung, B., Ribergaard, M., & Lyberth, B. (2008). Acceleration of jakobshavn isbr triggered by warm subsurface ocean waters [Journal Article]. *Nature Geoscience*, *1*, 659-664. doi: 10.1038/ngeo316

Holland, M. M., Bailey, D. A., Briegleb, B. P., Light, B., & Hunke, E. (2012). Improved sea ice shortwave radiation physics in ccsm4: The impact of melt ponds and aerosols on arctic sea ice [Journal Article]. *Journal of Climate*, *25*(5), 1413-1430. Retrieved from https://journals.ametsoc.org/view/journals/clim/25/5/jcli-d-11-00078.1.xml doi: 10.1175/jcli-d-11-00078.1

Holland, M. M., Bitz, C. M., & Tremblay, B. (2006). Future abrupt reductions in the summer arctic sea ice [Journal Article]. *Geophysical Research Letters*, *33*(23). Retrieved from https://agupubs.onlinelibrary.wiley.com/doi/abs/10.1029/2006GL028024 doi: https://doi.org/10.1029/2006GL028024

Hunke, E. C., & Dukowicz, J. K. (1997). An elastic–viscous–plastic model for sea ice dynamics [Journal Article]. *Journal of Physical Oceanography*, *27*(9), 1849-1867. Retrieved from https://journals.ametsoc.org/view/journals/phoc/27/9/1520-0485_1997_027_1849_aevpmf_2.0.co_2.xml doi: 10.1175/1520-0485(1997)027⟨1849:aevpmf⟩2.0.co;2

IPCC. (2013). Summary for policymakers [Book Section]. In T. Stocker et al. (Eds.), *Climate change 2013: The physical science basis. contribution of working group i to the fifth assessment report of the intergovernmental panel on climate change* (p. 1–30). Cambridge, United Kingdom and New York, NY, USA: Cambridge University Press. Retrieved from www.climatechange2013.org doi: 10.1017/CBO9781107415324.004

Jackson, L. C., Roberts, M. J., Hewitt, H. T., Iovino, D., Koenigk, T., Meccia, V. L., ... Wood, R. A. (2020). Impact of ocean resolution and mean state on the rate of amoc weakening [Journal Article]. *Climate Dynamics*, *55*(7), 1711-1732. Retrieved from https://doi.org/10.1007/s00382-020-05345-9 doi: 10.1007/s00382-020-05345-9

Jahn, A., Kay, J. E., Holland, M. M., & Hall, D. M. (2016). How predictable is the timing of a summer ice-free arctic? [Journal Article]. *Geophys. Res. Lett.*, *43*, 9113– 9120. doi: doi:10.1002/2016GL070067

Jansen, M. F., Adcroft, A. J., Hallberg, R., & Held, I. M. (2015). Parameterization of eddy fluxes based on a mesoscale energy budget [Journal Article]. *Ocean Modelling*, *92*, 28-41. Retrieved from https://www.sciencedirect.com/science/article/pii/S1463500315000967 doi: https://doi.org/10.1016/j.ocemod.2015.05.007

Kirtman, B. P., Bitz, C., Bryan, F., Collins, W., Dennis, J., Hearn, N., ... Vertenstein, M. (2012). Impact of ocean model resolution on ccsm climate simulations [Journal Article]. *Climate Dynamics*, *39*(6), 1303-1328. Retrieved from https://doi.org/10.1007/s00382-012-1500-3 doi: 10.1007/s00382-012-1500-3

Koenigk, T., Fuentes-Franco, R., Meccia, V. L., Gutjahr, O., Jackson, L. C., New, A. L., ... Sein, D. V. (2021). Deep mixed ocean volume in the labrador sea in highresmip models [Journal Article]. *Climate Dynamics*. Retrieved from https://doi.org/10.1007/s00382-021-05785-x doi: 10.1007/s00382-021-05785-x

Kurihara, Y., & Tripoli, G. J. (1976). An iterative time integration scheme designed to preserve a low-frequency wave [Journal Article]. *Monthly Weather Review*, *104*(6), 761-764. Retrieved from https://journals.ametsoc.org/view/journals/mwre/104/6/1520-0493_1976_104_0761_aitisd_2_0_co_2.xml doi: 10.1175/1520-0493(1976)104⟨0761:aitisd⟩2.0.co;2

Langehaug, H. R., Medhaug, I., Eldevik, T., & Otterå, O. H. (2012). Arctic/atlantic exchanges via the subpolar gyre [Journal Article]. *Journal of Climate*, *25*(7), 2421-2439. Retrieved from https://doi.org/10.1175/JCLI-D-11-00085.1 doi: 10.1175/JCLI-D-11-00085.1

Large, W. G., McWilliams, J. C., & Doney, S. C. (1994). Oceanic vertical mixing: A review and a model with a nonlocal boundary layer parameterization [Journal Article]. *Reviews of Geophysics*, *32*(4), 363-403. Retrieved from https://doi.org/10.1029/94RG01872 doi: https://doi.org/10.1029/94RG01872

Li, D., Zhang, R., & Knutson, T. R. (2017). On the discrepancy between observed and cmip5 multi-model simulated barents sea winter sea ice decline [Journal Article]. *Nature Communications*, *8*(1), 14991. Retrieved from https://doi.org/10.1038/ncomms14991 doi: 10.1038/ncomms14991

Marzocchi, A., Hirschi, J. J. M., Holliday, N. P., Cunningham, S. A., Blaker, A. T., & Coward, A. C. (2015). The north atlantic subpolar circulation in an eddy-resolving global ocean model [Journal Article]. *Journal of Marine Systems*, *142*, 126-143. Retrieved from https://www.sciencedirect.com/science/article/pii/S0924796314002437 doi: https://doi.org/10.1016/j.jmarsys.2014.10.007

Mette, M. J., Wanamaker Jr, A. D., Retelle, M. J., Carroll, M. L., Andersson, C., & Ambrose Jr, W. G. (2021). Persistent multidecadal variability since the 15th century in the southern barents sea derived from annually resolved shell-based records [Journal Article]. *Journal of Geophysical Research: Oceans*, *126*(6), e2020JC017074. Retrieved from https://agupubs.onlinelibrary.wiley.com/doi/abs/10.1029/2020JC017074 doi: https://doi.org/10.1029/2020JC017074

Milly, P. C. D., Malyshev, S. L., Shevliakova, E., Dunne, K. A., Findell, K. L., Gleeson, T., … Swenson, S. (2014). An enhanced model of land water and energy for global hydrologic and earth-system studies [Journal Article]. *Journal of Hydrometeorology*, *15*(5), 1739-1761. Retrieved from https://journals.ametsoc.org/view/journals/hydr/15/5/jhm-d-13-0162_1.xml doi: 10.1175/jhm-d-13-0162.1

Molinari, J., & Dudek, M. (1992). Parameterization of convective precipitation in mesoscale numerical models: A critical review [Journal Article]. *Monthly Weather Review*, *120*(2), 326-344. Retrieved from https://journals.ametsoc.org/view/journals/mwre/120/2/1520-0493_1992_120_0326_pocpim_2_0_co_2.xml doi: 10.1175/1520-0493(1992)120⟨0326:pocpim⟩2.0.co;2

Murray, R. J. (1996). Explicit generation of orthogonal grids for ocean models [Journal Article]. *Journal of Computational Physics*, *126*(2), 251-273. Retrieved from http://www.sciencedirect.com/science/article/pii/S0021999196901369 doi: https://doi.org/10.1006/jcph.1996.0136

Myers, P. G., Kulan, N., & Ribergaard, M. H. (2007). Irminger water variability in the west greenland current [Journal Article]. *Geophysical Research Letters*, *34*(17). Retrieved from https://doi.org/10.1029/2007GL030419 doi: https://doi.org/10.1029/2007GL030419

Notz, D., & SIMIP Community. (2020). Arctic sea ice in cmip6 [Journal Article]. *Geophysical Research Letters*, *47*(10), e2019GL086749. Retrieved from https://agupubs.onlinelibrary.wiley.com/doi/abs/10.1029/2019GL086749 doi: https://doi.org/10.1029/2019GL086749

Pacanowski, R., & Gnanadesikan, A. (1998). Transient response in a z-level ocean model that resolves topography with partial cells [Journal Article]. *Monthly Weather Review - MON WEATHER REV*, *126*. doi:

10.1175/1520-0493(1998)126⟨3248:TRIAZL⟩2.0.CO;2
Pennelly, C., & Myers, P. G. (2020). Introducing lab60: A 1/60° nemo 3.6 numerical simulation of the labrador sea [Journal Article]. *Geosci. Model Dev.*, *13*(10), 4959-4975. Retrieved from `https://gmd.copernicus.org/articles/13/4959/2020/` doi: 10.5194/gmd-13-4959-2020
Pickart, R. S. (2004). Shelfbreak circulation in the alaskan beaufort sea: Mean structure and variability. *Journal of Geophysical Research: Oceans*, *109*(C4). Retrieved from `https://agupubs.onlinelibrary.wiley.com/doi/abs/10.1029/2003JC001912` doi: https://doi.org/10.1029/2003JC001912
Polyakov, I., Pnyushkov, A., Alkire, M., Ashik, I., Baumann, T., Carmack, E., ... Yulin, A. (2017). Greater role for atlantic inflows on sea-ice loss in the eurasian basin of the arctic ocean [Journal Article]. *Science (New York, N.Y.)*, *356*. doi: 10.1126/science.aai8204
Saba, V. S., Griffies, S. M., Anderson, W. G., Winton, M., Alexander, M. A., Delworth, T. L., ... Zhang, R. (2016). Enhanced warming of the northwest atlantic ocean under climate change [Journal Article]. *Journal of Geophysical Research: Oceans*, *121*(1), 118-132. Retrieved from `https://agupubs.onlinelibrary.wiley.com/doi/abs/10.1002/2015JC011346` doi: https://doi.org/10.1002/2015JC011346
Schauer, U., & Beszczynska-Moeller, A. (2009). Problems with estimation and interpretation of oceanic heat transport - conceptual remarks for the case of fram strait in the arctic ocean [Journal Article]. *Ocean Science (OS)*, *5*. doi: 10.5194/os-5-487-2009
Semtner, A. J. (1976). A model for the thermodynamic growth of sea ice in numerical investigations of climate [Journal Article]. *Journal of Physical Oceanography*, *6*(3), 379-389. Retrieved from `https://journals.ametsoc.org/view/journals/phoc/6/3/1520-0485_1976_006_0379_amfttg_2_0_co_2.xml` doi: 10.1175/1520-0485(1976)006⟨0379:AMFTTG⟩2.0.CO;2
Shi, X., Notz, D., Liu, J., Yang, H., & Lohmann, G. (2020). Sensitivity of northern hemisphere climate to ice-ocean interface heat flux parameterizations [Journal Article]. *Geoscientific Model Development Discussions*, *2020*, 1–26. Retrieved from `https://gmd.copernicus.org/preprints/gmd-2020-287/` doi: 10.5194/gmd-2020-287
Smedsrud, L. H., Ingvaldsen, R., Nilsen, J. E. Ø., & Skagseth, Ø. (2010). Heat in the barents sea: transport, storage, and surface fluxes [Journal Article]. *Ocean Sci.*, *6*(1), 219-234. Retrieved from `https://os.copernicus.org/articles/6/219/2010/` doi: 10.5194/os-6-219-2010
Smith, M., Holland, M., & Light, B. (2021). Arctic sea ice sensitivity to lateral melting representation in a coupled climate model [Journal Article]. *The Cryosphere Discuss.*, *2021*, 1-21. Retrieved from `https://tc.copernicus.org/preprints/tc-2021-67/` doi: 10.5194/tc-2021-67
Straneo, F., & Heimbach, P. (2013). North atlantic warming and the retreat of greenland's outlet glaciers [Journal Article]. *Nature*, *504*(7478), 36-43. Retrieved from `https://doi.org/10.1038/nature12854` doi: 10.1038/nature12854
Stroeve, J. C., Kattsov, V., Barrett, A., Serreze, M., Pavlova, T., Holland, M., & Meier, W. N. (2012). Trends in arctic sea ice extent from cmip5, cmip3 and observations [Journal Article]. *Geophysical Research Letters*, *39*(16). Retrieved from `https://agupubs.onlinelibrary.wiley.com/doi/abs/10.1029/2012GL052676` doi: https://doi.org/10.1029/2012GL052676
Stroeve, J. C., Markus, T., Boisvert, L., Miller, J., & Barrett, A. (2014). Changes in arctic melt season and implications for sea ice loss [Journal Article]. *Geophysical Research Letters*, *41*(4), 1216-1225. Retrieved from `https://agupubs.onlinelibrary.wiley.com/doi/abs/10.1002/2013GL058951` doi: https://doi.org/10.1002/2013GL058951

Strong, C., Magnusdottir, G., & Stern, H. (2009). Observed feedback between winter sea ice and the north atlantic oscillation [Journal Article]. *Journal of Climate*, *22*(22), 6021-6032. Retrieved from `https://doi.org/10.1175/2009JCLI3100.1` doi: 10.1175/2009JCLI3100.1

Timmermans, M.-L., & Marshall, J. (2020). Understanding arctic ocean circulation: A review of ocean dynamics in a changing climate [Journal Article]. *Journal of Geophysical Research: Oceans*, *125*(4), e2018JC014378. Retrieved from `https://agupubs.onlinelibrary.wiley.com/doi/abs/10.1029/2018JC014378` doi: 10.1029/2018jc014378

Tsamados, M., Feltham, D., Petty, A., Schroeder, D., & Flocco, D. (2015). Processes controlling surface, bottom and lateral melt of arctic sea ice in a state of the art sea ice model [Journal Article]. *Philosophical Transactions of the Royal Society A: Mathematical, Physical and Engineering Sciences*, *373*(2052), 20140167. Retrieved from `https://royalsocietypublishing.org/doi/abs/10.1098/rsta.2014.0167` doi: doi:10.1098/rsta.2014.0167

Ungermann, M., Tremblay, L. B., Martin, T., & Losch, M. (2017). Impact of the ice strength formulation on the performance of a sea ice thickness distribution model in the arctic [Journal Article]. *Journal of Geophysical Research: Oceans*, *122*(3), 2090-2107. Retrieved from `https://agupubs.onlinelibrary.wiley.com/doi/abs/10.1002/2016JC012128` doi: https://doi.org/10.1002/2016JC012128

Venegas, S., & Mysak, L. (2000, 10). Is there a dominant timescale of natural climate variability in the arctic? *Journal of Climate - J CLIMATE*, *13*, 3412-3434. doi: 10.1175/1520-0442(2000)013⟨3412:ITADTO⟩2.0.CO;2

Walsh, J. E., Chapman, W. L., Fetterer, F., & Stewart, J. S. (2019). *Gridded monthly sea ice extent and concentration, 1850 onward, version 2.* (Boulder, Colorado USA. NSIDC: National Snow and Ice Data Center. Data accessed 06/2021) doi: 10.7265/jj4s-tq79

Winton, M. (2000). A reformulated three-layer sea ice model [Journal Article]. *Journal of Atmospheric and Oceanic Technology*, *17*(4), 525-531. Retrieved from `https://journals.ametsoc.org/view/journals/atot/17/4/1520-0426_2000_017_0525_artlsi_2_0_co_2.xml` doi: 10.1175/1520-0426(2000)017⟨0525:artlsi⟩2.0.co;2

Woodgate, R. A., Weingartner, T., & Lindsay, R. (2010). The 2007 bering strait oceanic heat flux and anomalous arctic sea-ice retreat [Journal Article]. *Geophysical Research Letters*, *37*(1). Retrieved from `https://agupubs.onlinelibrary.wiley.com/doi/abs/10.1029/2009GL041621` doi: 10.1029/2009gl041621

Yamamoto-Kawai, M., McLaughlin, F. A., Carmack, E. C., Nishino, S., & Shimada, K. (2008). Freshwater budget of the canada basin, arctic ocean, from salinity, δ18o, and nutrients. *Journal of Geophysical Research: Oceans*, *113*(C1). Retrieved from `https://agupubs.onlinelibrary.wiley.com/doi/abs/10.1029/2006JC003858` doi: https://doi.org/10.1029/2006JC003858